MULTISCALE MODEL. SIMUL.
Vol. 6, No. 4, pp. 1169–1197

HYBRID MULTISCALE METHODS II. KINETIC EQUATIONS*

GIACOMO DIMARCO† AND LORENZO PARESCHI†

Abstract. In this work we consider the development of a new family of hybrid numerical methods for the solution of kinetic equations which involves different scales. The basic idea is to couple macroscopic and microscopic models in all cases in which the macroscopic model does not provide correct results. The key aspect in the development of the algorithms is the choice of a suitable hybrid representation of the solution and a merging of Monte Carlo methods in nonequilibrium regimes with deterministic methods in equilibrium ones. This approach permits us to treat efficiently both the microscopic and the macroscopic scales. Applications to the Boltzmann–BGK equation are presented to show the performance of the new methods.

Key words. multiscale methods, Boltzmann equation, Euler equation, fluid-dynamic limit, Monte Carlo methods, kinetic schemes

AMS subject classifications. 65M99, 65L06, 82D05

DOI. 10.1137/070680916

1. Introduction.

A broad range of scientific problems involve multiple scales and multiscale phenomena (material science, chemistry, fluid dynamics, biology, ...). Examples are microscopic departures from macroscopic neutrality in plasmas, dislocation in plastic deformation, turbulence in fluid, or molecular reaction in biology simulations. These phenomena involve different physical laws which govern the processes at different scales. In many situations we are interested only in the macroscopic scale of the problems, and we would like to have equations to describe these macroscopic variables, ignoring the rest. From the computational point of view, the representation of the solution through the microscopic model has an overwhelming cost. To this aim many numerical methods have been developed which address explicitly the multiscale structure of the solution such as wavelet [19], domain decomposition in space [3, 4, 12, 11, 25, 14] and in space velocity [9], stiff solvers [5, 20, 21, 22], and adaptive mesh refinement [7, 32]. In addition, coupling techniques for a microscopic stochastic solver with a macroscopic deterministic model for ODEs or PDEs [16, 17, 18, 23, 24, 34] gave very good results in the recent past. In the present work we afford in details the problem in the case of multiscale kinetic equations. The Navier–Stokes or the Euler equations, which describe the problem at the macroscopic level, do not give a satisfactory description of the physical system in all situations, and a kinetic description through the Boltzmann equation is often required. The development of numerical methods to solve rarefied gas dynamics (RGD) problems is a big challenge due to the presence of different time and/or space scales. As a consequence the dominant methods for the computations are based on probabilistic Monte Carlo techniques at different levels [2, 27, 30]. They have many advantages in terms of computational cost for problems with high dimensions: simplicity in preserving some physical properties of the underlying problem (typically using a particle interpretation

*Received by the editors January 25, 2007; accepted for publication (in revised form) June 7, 2007; published electronically January 11, 2008. This work was partially supported by the European network HYKE, funded by the EC as contract HPRN-CT-2002-00282, and by the project NUMSTAT funded by the University of Ferrara.

http://www.siam.org/journals/mms/6-4/68091.html

†Department of Mathematics, University of Ferrara, Ferrara 44100, Italy (Giacomo.Dimarco@unife.it, Lorenzo.Pareschi@unife.it).

of the statistical sample) and great flexibility when dealing with complicated geometries. On the other hand, particle methods yield low accurate and fluctuating results with respect to deterministic methods, and the convergence, in general, is quite low. Typically, in continuum regions a macroscopic numerical scheme that solves the Euler or the Navier–Stokes equations gives the correct results. Thus it is highly desirable to have a method that combines a Monte Carlo solver in nonequilibrium regions with a deterministic solver in equilibrium ones. Domain decomposition techniques are then often used in order to better treat these difficulties and to design suitable numerical schemes. However, this multimodeling approach requires the a priori knowledge of some of the scales, in order to define the different regions where the different models are valid, which are typically hard to know in practice [3, 25, 10].

In this paper we will focus on the Boltzmann–BGK model, which is known to be accurate in describing systems close to equilibrium [8]. First, we extend the results obtained in [13] for the solution of systems of hyperbolic equations with relaxation to the case of kinetic equations. Next, we propose several generalizations to the multiscale hybrid schemes in order to afford the new complications that arise in the simulation of multiscale RGD, such as the lack of a compact support for the probability distribution function in velocity space.

The strategy is based on the solution of the full model in the whole computational domain and on the design of the numerical method in such a way that it is capable of taking advantage of the model reduction when we approach the thermodynamic equilibrium. This involves the development of heterogeneous numerical methods which hybridize different numerical approaches of probabilistic and deterministic nature.

The main features of the schemes can be summarized as follows:

(i) In regions far from equilibrium, where the solution of the full kinetic equation is required, the schemes provide a probabilistic Monte Carlo approximation of the solution.

(ii) In thermodynamic equilibrium regions, where the Euler equations are valid, the schemes provide a deterministic finite volume/difference approximation without any time step restrictions induced by the small relaxation rate.

(iii) In intermediate regions, the approximated solution is generated automatically by the schemes as a suitable blending of a nonequilibrium probabilistic component and an equilibrium deterministic one.

The rest of the article is organized as follows. First, we introduce the Boltzmann–BGK equation and its main properties. Then we present the hybrid schemes with particular emphasis on the difference between solving the true Boltzmann–BGK equation (which is not compactly supported in velocity space) and a discrete velocity model (for which we need an artificial boundary in velocity space). Next, in section 4 we perform several numerical tests in order to compare the different performances of the methods. Some final considerations are reported in the last section.

2. Boltzmann–BGK equation. We consider the Boltzmann–BGK equation

$$\partial_t f + v \cdot \nabla_x f = \frac{1}{\tau}(M_f - f), \tag{1}$$

with the initial condition

$$f(x, v, t = 0) = f_0(x, v), \tag{2}$$

where $f = f(x, v, t)$ is a nonnegative function describing the time evolution of the distribution of particles which move with velocity $v \in \mathbb{R}^{d_x}$, in the position $x \in \Omega \subset \mathbb{R}^{d_v}$

at time $t > 0$. In most applications $d_x = d_v = 3$; however, one-dimensional and two-dimensional models are often used.

The relaxation time τ is defined in the dimensional case as [1]

$$\tau^{-1} = A_c \varrho, \tag{3}$$

where A_c is a constant and ϱ is the density. In [12] the relaxation parameter is defined as

$$\tau^{-1} = C \varrho T^{1-\omega}, \tag{4}$$

where T is the temperature, while ω and C are constants that depend on the gas. In the adimensional case we have

$$\tau^{-1} = \frac{C_1}{\varepsilon}. \tag{5}$$

The parameter $\varepsilon > 0$ is the Knudsen number and is proportional to the mean free path between collision, while C_1 is a constant that we choose equal to one [8, 33]. In the BGK equation the collisions are modeled with a relaxation towards the equilibrium M_f called Maxwellian. The local Maxwellian function is defined by

$$M_f(\varrho, u, T)(v) = \frac{\varrho}{(2\pi T)^{3/2}} \exp\left(\frac{-|u-v|^2}{2T}\right), \tag{6}$$

where ϱ, u, and T are the density, mean velocity, and temperature of the gas,

$$\varrho = \int_{\mathbb{R}^3} f dv, \quad u = \int_{\mathbb{R}^3} v f dv, \quad T = \frac{1}{3\varrho} \int_{\mathbb{R}^3} |v-u|^2 f dv, \tag{7}$$

while the energy E is defined as

$$E = \frac{1}{2} \int_{\mathbb{R}^3} |v|^2 f dv. \tag{8}$$

Finally, we define the kinetic entropy of f by

$$H_f = \int_{\mathbb{R}^3} f \log f dv. \tag{9}$$

Now, if we consider the BGK equation (1) and multiply it for 1, v, $\frac{1}{2}|v^2|$, the so-called collision invariant, by integrating in v we obtain the first three moments of the distribution function f:

$$\begin{aligned}
&\frac{\partial \varrho}{\partial t} + \sum_{i=1}^{3} \frac{\partial}{x_i}(\varrho u_i) = 0, \\
&\frac{\partial \varrho u_j}{\partial t} + \sum_{i=1}^{3} \frac{\partial}{x_i}(\varrho u_i u_j + p_{ij}) = 0, \qquad j = 1,2,3, \\
&\frac{\partial}{\partial t}\left(\frac{1}{2}\varrho|u|^2 + \varrho e\right) + \sum_{i=1}^{3} \frac{\partial}{\partial x_i}\left[\varrho u_i \left(\frac{1}{2}|u|^2 + e\right) + \sum_{i=1}^{3} u_i p_{ij} + q_i\right] = 0.
\end{aligned} \tag{10}$$

These equations are the corresponding conservations laws for mass, momentum, and energy, in which e represents the internal energy and p the kinetic pressure, while

q is the third order moment. Furthermore, the dissipation of entropy could easily be proved:

$$\partial_t \int f \log f dv + \nabla_x \int v f \log f dv \leq 0. \tag{11}$$

Unfortunately the differential system of equations (10) is not closed, since it involves higher order moments of the distribution function. Now it can be seen that M_f is the unique solution of the following entropy minimization problem:

$$H_{M_f} = \min \left\{ H_f,\ f \geq 0 \text{ s.t. } \int_{\mathbb{R}^3} \mathbf{m} f = \boldsymbol{\varrho} \right\}, \tag{12}$$

where $\mathbf{m}$ is the vector containing the collision invariants, while $\boldsymbol{\varrho}$ is the vector containing the first three moments of f:

$$\mathbf{m}(v) = \left(1, v, \frac{1}{2}|v|^2\right), \qquad \boldsymbol{\varrho} = (\varrho, \varrho u, E). \tag{13}$$

This is the well-known Boltzmann *H-theorem*, and it means that the local equilibrium state minimizes the entropy of all the possible states leading to the same macroscopic properties. Now formally as $\varepsilon \to 0$ the function f tends to Maxwellian. In this case it is possible to compute f from its moments, thus obtaining the closed Euler system of compressible gas dynamics equations:

$$\begin{aligned} &\frac{\partial \varrho}{\partial t} + \nabla_x \cdot (\varrho u) = 0, \\ &\frac{\partial \varrho u}{\partial t} + \nabla_x \cdot (\varrho u \otimes u + p) = 0, \\ &\frac{\partial E}{\partial t} + (Eu + pu) = 0, \\ &p = \varrho T, \qquad E = \frac{3}{2}\varrho T + \frac{1}{2}\varrho |u|^2. \end{aligned} \tag{14}$$

2.1. Boundary conditions. Typically, (1) is completed with boundary conditions for $x \in \partial\Omega$ and for $v \cdot n \geq 0$, where n denotes the unit normal, pointing inside the domain. The boundary conditions are modeled by

$$|v \cdot n| f(x, v, t) = \int_{v_* \cdot n < 0} |v_* \cdot n| K(v_* \to v, x, t) f(x, v_*, t) dv_*, \tag{15}$$

where v_* is the velocity after the process. The entering flux is described as a function of the outgoing flux modified by the boundary kernel K. Such a definition of the boundary condition preserves the mass if

$$K(v_* \to v, x, t) \geq 0, \qquad \int_{v_* \cdot n \geq 0} K(v_* \to v, x, t) dv = 1. \tag{16}$$

Usually we apply two types of boundary conditions, absorbing or reflecting; another condition could be a convex combination of the two. From a physical point of view, one assumes that a fraction of particle (α) is absorbed and reemitted at a temperature and velocity corresponding to a Maxwellian (with temperature and velocity of the

boundary), while the other $(1-\alpha)$ is specular reflected; this is equivalent to imposing for the ingoing velocities

$$f(x,v,t) = (1-\alpha) * Rf(x,v,t) + \alpha Mf(x,v,t), \qquad v \cdot n(x) \geq 0, \tag{17}$$

and

$$\begin{aligned} Rf(x,v,t) &= f(x, v - 2n(n\cdot v), t), \\ Mf(x,v,t) &= \mu(x,t) M_\omega(v,t). \end{aligned} \tag{18}$$

If we denote by T_ω the temperature of the boundary and by u_ω the velocity, M_ω is given by

$$M_\omega(\varrho, u_\omega, T_\omega)(v) = \frac{\varrho}{(2\pi T_w)^{3/2}} \exp\left(\frac{-|u_w - v|^2}{2T_w}\right). \tag{19}$$

Finally, the value of μ is determined by mass conservation:

$$\mu(x,t) \int_{v\cdot n \geq 0} M_\omega(v)|v\cdot n| dv = \int_{v\cdot n<0} f(x,v,t)|v\cdot n| dv. \tag{20}$$

We note that for $\alpha = 0$ (specular reflection) the reemitted particles have the same flow of mass, temperature, and tangential momentum of the incoming molecules, while for $\alpha = 1$ (full accommodation) the reemitted particles have completely lost memory of the incoming values (only the global mass is conserved).

3. Hybrid methods. In what follows we will restrict ourselves for the sake of simplicity to the one-dimensional situation $d_x = d_v = 1$, even though our methods apply naturally to the full three-dimensional case. Furthermore, the dependence on the x and t variables will be omitted in this introductory part.

The starting point in the construction of all the hybrid methods is the interpretation of the distribution function as a probability density,

$$f(v) \geq 0, \qquad \varrho = \int_{-\infty}^{+\infty} f(v) dv = 1, \tag{21}$$

and the following definition of hybrid representation.

DEFINITION 1. *Given a probability density $f(v)$, and a probability density $M(v)$, called equilibrium density, we define $w(v) \in [0,1]$ and $\tilde{f} \geq 0$ in the following way:*

$$w(v) = \begin{cases} \dfrac{f(v)}{M(v)}, & f(v) \leq M(v) \neq 0, \\ 1, & f(v) \geq M(v) \end{cases} \tag{22}$$

and

$$\tilde{f}(v) = f(v) - w(v) M(v). \tag{23}$$

Thus $f(v)$ can be represented as (Figure 1, left)

$$f(v) = \tilde{f}(v) + w(v) M(v). \tag{24}$$

If we now take

$$\beta = \min_v \{w(v)\} \tag{25}$$

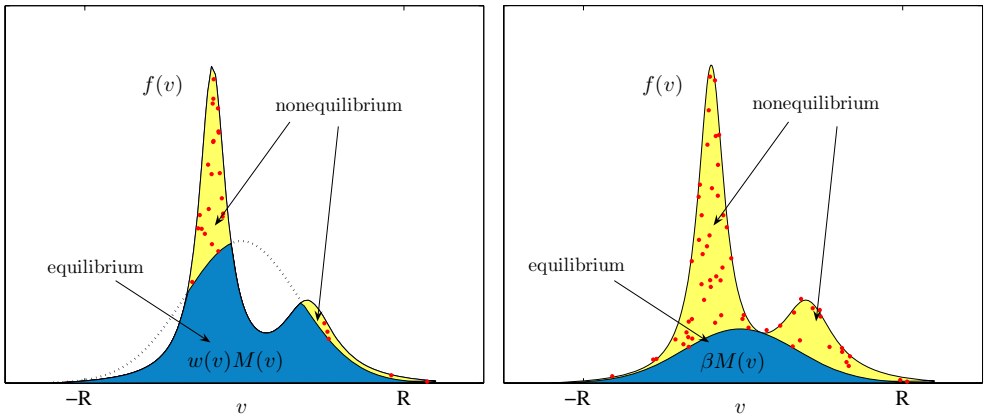

FIG. 1. *Distribution function as a combination of equilibrium and nonequilibrium part representation* (24) *left,* (28) *right.*

and

$$\tilde{f}(v) = f(v) - \beta M(v), \tag{26}$$

we have

$$\int_v \tilde{f}(v)dv = 1 - \beta. \tag{27}$$

Let us define for $\beta \neq 1$ the probability density

$$f^p(v) = \frac{\tilde{f}(v)}{1-\beta}.$$

The case $\beta = 1$ is trivial since it implies $f(v) = M(v)$. Thus the probability density $f(v)$ can be written as a convex combination of two probability densities in the form [28, 29] (Figure 1, right)

$$f(v) = (1-\beta)f^p(v) + \beta M(v). \tag{28}$$

Clearly the above representation is a particular case of (24).

REMARK 1. *If we define for* $R > 0$

$$w_R(v) = \begin{cases} w(v), & |v| \leq R, \\ 0, & |v| > R \end{cases} \tag{29}$$

and

$$\tilde{f}_R(v) = \begin{cases} \tilde{f}(v), & |v| \leq R, \\ f(v), & |v| > R, \end{cases} \tag{30}$$

we have the representation

$$f(v) = \tilde{f}_R(v) + w_R(v)M(v). \tag{31}$$

In this case taking

$$\beta_R = \min_v\{w_R(v)\} \geq \beta \tag{32}$$

and

$$\tilde{f}_R(v) = f(v) - \beta_R E(v), \tag{33}$$

where $E(v) = M(v)\Psi(|v| \le R)$ *and* $\Psi(\cdot)$ *is the indicator function, we have*

$$\int_v \tilde{f}_R(v)dv = 1 - \rho_E\beta_R, \qquad \rho_E = \int E(v)dv \le 1. \tag{34}$$

Let us define the probability density

$$f_R^p(v) = \frac{\tilde{f}_R(v)}{1 - \rho_E\beta_R}.$$

Again $f(v)$ *can be written as a convex combination of two probability densities in the form*

$$f(v) = (1 - \rho_E\beta_R)f_R^p(v) + \rho_E\beta_R\frac{E(v)}{\rho_E}. \tag{35}$$

Of course these representations are particularly useful since, as we will see in what follows, they allow us to restrict the deterministic part of the schemes to compactly supported function in velocity space.

For a more general function which depends also on space and time we consider the following representation:

$$f(x,v,t) = \underbrace{\tilde{f}(x,v,t)}_{nonequilibrium} + \underbrace{w(x,v,t)\,M(x,v,t)}_{equilibrium},$$

where $w(x,v,t)$ is a continuum function (which may or may not be compactly supported in v) that characterizes the equilibrium fraction and $\tilde{f}(x,v,t)$ the nonequilibrium part of the distribution function. In order to compute the solution we need to discretize the velocity space; thus practically the function $w(x,v,t)$ becomes the approximation $w_k(x,t) = w(x,v_k,t)$, which means we replace our continuous function by a piecewise constant function. The general methodology consists in the following:

(i) Solve the evolution of the perturbation by Monte Carlo methods. Thus $\tilde{f}(x,v,t)$ will be represented by a set of samples in the computational domain.

(ii) Solve the evolution of the equilibrium fraction by deterministic methods. Thus $w(x,v,t)\,M(x,v,t)$ will be represented on a suitable grid in the computational domain.

In what follows we will describe the different schemes. In the first part we start from a discrete velocity model (DVM) of the Boltzmann–BGK equation. Thus the velocity space is naturally discretized and bounded by the model itself, and the schemes we obtain in this case represent a direct generalization of [13]. In the second part we show how to extend our methodology to the full Boltzmann–BGK equation without any artificial boundary in the velocity space.

3.1. Hybrid DVM-BGK schemes. In order to introduce the reader to the main tools used, we first describe briefly a DVM-BGK scheme and how to solve it with a fully deterministic and a fully Monte Carlo method.

3.1.1. DVM-BGK. We assume that gas particles can attain only a finite set of velocities (see [26] for details about DVM-BGK models). Let $\mathcal{K}$ be a set of N multi-indexes, defined by $\mathcal{K} = \{k = (k^i)_{i=1}^D,\ k^i \le K^i\}$, where $D = 1, 2, 3$ is the space dimension and $\{K^i\}$ are given bounds. The set of possible velocities reads

$$\mathcal{V} = \{v_k = k\triangle v + a,\ k \in \mathcal{K}\}, \tag{36}$$

where a is an arbitrary vector of $\mathbb{R}^D$ and $\triangle v$ is a scalar. We denote the discrete collision invariants by $\mathbf{m}_k = (1, v_k, \frac{1}{2}|v_k|^2)$, and the continuous distribution function becomes a piecewise constant function $f_{\mathcal{K}}(t,x) = (f_k(t,x))_{k\in\mathcal{K}}$, where each component $f_k(t,x)$ is assumed to be an approximation of $f(x, v_k, t)$. The macroscopic quantities are now given by sums on $\mathcal{V}$:

$$\boldsymbol{\varrho}_{\mathcal{K}}(t,x) = \sum_{k\in\mathcal{K}} \mathbf{m}_k f_k(t,x), \tag{37}$$

$$H_{\mathcal{K}}(t,x) = \sum_{k\in\mathcal{K}} f_k(t,x)\log f_k(t,x). \tag{38}$$

The solution of the BGK model is reduced to the solution of a set of N equations:

$$\partial_t f_k + v_k\cdot\nabla_x f_k = \frac{1}{\varepsilon}(\mathcal{E}_k - f_k) \qquad \forall k \in \mathcal{K}. \tag{39}$$

Now the main problem is to define an approximation $\mathcal{E}_{f_{\mathcal{K}}}$ of the Maxwellian equilibrium $M_{f_{\mathcal{K}}}$ such that conservation is preserved (10) and dissipation of entropy is assured (11). Notice that the natural approximation $\mathcal{E}_k = M_{f_{\mathcal{K}}}(v_k)$ cannot satisfy these requirements. Let us define $\mathcal{E}_{\mathcal{K}}$ by the minimum of discrete entropy among all the piecewise constant functions, defined on the same support and with the same discretization of the velocity space, that have the same moments of f:

$$H_{\mathcal{E}_{\mathcal{K}}} = \min\left\{H_g,\ g \ge 0 \text{ s.t. } \sum_{k\in\mathcal{K}} \mathbf{m}_k g_k = \boldsymbol{\varrho}_{\mathcal{K}}\right\}. \tag{40}$$

It has been proved that the solution for this problem exists; it is unique and has an exponential form [26]. Due to the above results, the computation of $\mathcal{E}_{\mathcal{K}}$ can be obtained through the solution of the nonlinear set of equations for $\boldsymbol{\alpha}$:

$$\sum_{k\in\mathcal{K}} \mathbf{m}_k \exp(\boldsymbol{\alpha}\cdot\mathbf{m}_k) = \boldsymbol{\varrho}_{\mathcal{K}}. \tag{41}$$

This nonlinear set of equations can be solved, for instance, by a Newton algorithm. The parameters $\boldsymbol{\alpha}$ are functions of t and x and can be expressed in terms of the macroscopic variables ϱ, u, T through

$$\boldsymbol{\alpha} = \left(\log\left(\frac{\varrho}{(2\pi RT)^{\frac{3}{2}}} - \frac{|u|^2}{2RT}\right), \frac{u}{RT}, -\frac{1}{RT}\right). \tag{42}$$

Now let f_0 be a vector of $\mathbb{R}^N$; if the problem (39) has a solution $f_{\mathcal{K}}$, then we have

$$f_k(t,x) > 0 \qquad \forall\ k,t,x, \tag{43}$$

$$\mathcal{E}_k = \exp(\boldsymbol{\alpha}\cdot\mathbf{m}_k) \qquad \forall k, \tag{44}$$

$$\partial_t \sum_{k\in\mathcal{K}} \mathbf{m}_k f_k + \nabla_x \cdot \sum_{k\in\mathcal{K}} \mathbf{m}_k v_k f_k = 0, \tag{45}$$

$$\partial_t \sum_{k\in\mathcal{K}} f_k \log f_k + \nabla_x \cdot \sum_{k\in\mathcal{K}} v_k f_k \log f_k \le 0. \tag{46}$$

3.1.2. A deterministic numerical scheme for DVM-BGK. We restrict the presentation of the scheme to one spatial dimension and one velocity dimension on a Cartesian grid (see [26] and [33] for details about DVM-BGK deterministic numerical schemes). The equations to be solved are

$$\partial_t f_k + v_k \cdot \nabla_x f_k = \frac{1}{\varepsilon}(\mathcal{E}_k - f_k) \qquad \forall k \in \mathcal{K}. \tag{47}$$

Consider a spatial Cartesian uniform grid defined by nodes $x_i = (i\triangle x)$ and a time discretization $t_n = n\triangle t$. Thus $f^n_{k,i}$ is an approximation of $f(t_n, x_i, v_k)$ inside the space cell $I =]x_{i-\frac{1}{2}}, x_{i+\frac{1}{2}}[$, and the corresponding discrete equilibrium is denoted by $\mathcal{E}^n_i = (\mathcal{E}^n_{k,i})_{k\in\mathcal{K}}$, and is therefore $\mathcal{E}^n_{k,i} = \exp(\boldsymbol{\alpha}^n_i \cdot \mathbf{m}_k)$, where $\boldsymbol{\alpha}^n_i$ is the unique solution of the nonlinear set of equations

$$\sum_{k\in\mathcal{K}} \mathbf{m}_k \exp(\boldsymbol{\alpha}^{\boldsymbol{n}}_{\boldsymbol{i}} \cdot \mathbf{m}_k) = \boldsymbol{\varrho}^n_i. \tag{48}$$

The computation of $\boldsymbol{\alpha}^{\boldsymbol{n}}_{\boldsymbol{i}}$ is performed through a Newton algorithm with the choice of $\mathcal{E}^n_{k,i} = M_f(x_i, v_k, t_n)\ \forall k \in \mathcal{K}$ as initial value; in the cases tested the convergence of the method is fast: very often only one iteration is needed. However, if the choice of the boundary in velocity space is done wisely, $\mathcal{E}^n_{k,i}$ can approach $M_f(x_i, v_k, t_n)\ \forall k \in \mathcal{K}$.

Now, in order to introduce the hybrid scheme, we split the problem into a relaxation step and a convection step; the transport part is simply the linear convection equation and can be approximated by a standard finite volume scheme, while the relaxation step is represented by a system of stiff ODEs. The scheme reads

$$f^c_{k,i} = f^n_{k,i} - \frac{\Delta t}{\Delta x}\left(\mathcal{F}^n_{k,i+1/2} - \mathcal{F}^n_{k,i-1/2}\right) \qquad \forall k \in \mathcal{K}, \tag{49}$$

where c indicates the intermediate step after the transport. The numerical fluxes are defined by

$$\mathcal{F}^n_{k,i+1/2} = \frac{1}{2}\left(v_k f^n_{k,i+1} + v_k f^n_{k,i} - |v_k|(f^n_{k,i+1} - f^n_{k,i})\right) \qquad \forall k \in \mathcal{K}. \tag{50}$$

For the relaxation step we utilize the exact solution of the ODE equation

$$f^r_{k,i} = e^{-\frac{\Delta t}{\varepsilon}} f^c_{k,i} + (1 - e^{-\frac{\Delta t}{\varepsilon}})\mathcal{E}^c_{k,i} \qquad \forall k \in \mathcal{K}, \tag{51}$$

where $\mathcal{E}^c_{k,i}$ is the discrete equilibrium function computed with the moments found after the convection. The distribution function at the next time step is simply $f^{n+1}_{i,k} = f^r_{i,k}$ $\forall k \in \mathcal{K}$. Finally, the time step is computed through the relation

$$\Delta t \left(\max_{\mathcal{K}}\left(\frac{|v_k|}{\Delta x}\right)\right) < 1. \tag{52}$$

3.1.3. A Monte Carlo scheme for DVM-BGK. A Monte Carlo approach to solve the DVM-BGK equations is the next tool we need for the construction of the hybrid schemes. In this model the distribution function is again represented by a piecewise constant function, defined on a compact support. We describe the scheme in one dimension in space and one dimension in space velocity. First, we split the equations into two parts, a transport and a relaxation stage:

$$\partial_t f^c_k(x,t) + v_k \cdot \nabla_x f^c_k(x,t) = 0 \qquad \forall k \in \mathcal{K}, \tag{53}$$

$$\partial_t f^r_k(x,t) = -\frac{1}{\varepsilon}(f^r_k(x,t) - \mathcal{E}^r_k(x,t)) \qquad \forall k \in \mathcal{K}. \tag{54}$$

The solution of the relaxation problem can be sought in the form of an evolution of a discrete probability density in each space point:

$$p_k(x,t) = \begin{cases} \dfrac{f_k(x,t)\Delta v}{\varrho(x,t)}, & v = v(k) \quad \forall k \in \mathcal{K}. \end{cases} \tag{55}$$

Thus, with probability $p_k(x,t)$, we assign to a sample velocity v_k. In order to begin the procedure we need to sample from the discrete probability density defined by the initial data $f_k^0(x,t)$. We want to sample N particles for each interval in the discrete space. We use the following strategy: divide the interval $[0,1]$ into K intervals, the ith interval being of length p_k, extract a uniform $[0,1]$ random number ξ, detect the interval k to which ξ belongs, and give to the sample velocity v_k. We can proceed as follows for each interval.

ALGORITHM 1 (discrete sampling).

1. *Compute* $P_k = \sum_{i=1}^{k} p_k$, $k = 1, .., K$, $P_0 = 0$.
2. *Find the integer* k *such that* $P_{k-1} \le \xi < P_k$, *with* ξ *a random number in* $[0,1]$.

Once P has been computed, step 2 can be performed with a binary search in $O(\ln K)$. Let us define with $\{\nu_1, \nu_2, \dots, \nu_N\}$ the initial samples from $p_{k,i}^0$ at a given space point x_i. Hence a Monte Carlo method to obtain samples from $p_{k,i}^n$ with n time step and ϱ_i solutions of the transport step is the following algorithm.

ALGORITHM 2 (Monte Carlo for DVM-BGK equations).

1. *Given* N *samples* ν_k, *the following hold:*
   (a) *With probability* $e^{-t/\varepsilon}$ *the samples are unchanged.*
   (b) *With probability* $1 - e^{-t/\varepsilon}$ *the samples are replaced with equilibrium samples. To extract* N *equilibrium samples proceed as follows:*
      i. *Compute* $p_{k,i} = \dfrac{\mathcal{E}_{k,i}^r \Delta v}{\varrho_i}$.
      ii. *Use* ***Algorithm 1***.

Here $\mathcal{E}_{k,i}^r$ represent the discrete equilibrium function at point x_i, computed with the moments found after convection. Note that the above procedure requires the exact knowledge of ϱ_i, which we can estimate only from the samples at the given point x_i. In practice we need the knowledge of density, mean velocity, and temperature at each point x_i to reconstruct the discrete Maxwellian. The simplest method, which produces a piecewise constant reconstruction, is based on evaluating the histogram of the samples on the grid. Given a set of N samples with position $\chi_1, \chi_2, \dots, \chi_N$ and velocity $\nu_1, \nu_2, \dots, \nu_N$, we define the discrete probability density at the cell centers:

$$p_k(x_i) = \frac{1}{N} \sum_{j=1}^{N} \Psi_{\Delta x}(\chi_j - x_i) \Phi_{\Delta v}(\nu_j - v_k), \qquad i,k = \dots, -2, -1, 0, 1, 2, \dots, \tag{56}$$

where $\Psi_{\Delta x}(x) = 1$ if $|x| \le \Delta x/2$ and $\Psi_{\Delta x}(x) = 0$ elsewhere, while $\Phi_{\Delta v}(v) = 1$ if $|v| \equiv 0$ and $\Phi_{\Delta v}(v) = 0$ in other cases.

Let us denote by the index k the sample ν_k and its position χ_k. If we use equations (56), then ϱ_i is given by the number of samples N_j belonging to the cell I_i:

$$\varrho_i = \frac{m}{\Delta x} \sum_{\chi_k \in I_i} 1 = \frac{m}{\Delta x} N_j, \tag{57}$$

where $m = \frac{1}{N} \int \varrho dx$, while the mean velocity and the energy are given by

$$u_i = \frac{1}{N_j} \sum_{\chi_k \in I_i} \nu_k, \qquad E_i = \frac{1}{2N_j} \frac{m}{\Delta x} \sum_{\chi_k \in I_i} |\nu_k|^2. \tag{58}$$

We refer the reader to [31] (and the references therein) for an introduction to basic sampling and different reconstruction techniques in Monte Carlo methods.

Finally, the transport step does not present any difficulty and can be applied without any need of meshes or reconstructions. In fact, from the exact expression of the solution $f^c_{k,i} = f^r_{k,i}(x - v_k t, t)\ \forall k \in \mathcal{K}$, we simply need to shift the position of the samples accordingly to the law

$$\chi_k = \chi_k + \nu_k t \qquad \forall k. \tag{59}$$

In what follows we will use the terminology "particle" to denote the pair (χ_k, ν_k) characterizing the sample ν_k and its position χ_k.

The method described above deserves some remarks.

REMARK 2.

(i) *One important aspect in the method is that we do not need to reconstruct the functions $f_{\mathcal{K}}$ but only the conserved quantity ϱ, u, T.*

(ii) *As for the deterministic DVM-BGK scheme, the Monte Carlo scheme presented needs the computation of a discrete equilibrium function through some iterative solver, such as the Newton method.*

(iii) *Note that as $\varepsilon \to 0$ the method becomes a Monte Carlo algorithm for the limiting fluid dynamic equations. This limiting method is the analogue of a kinetic particle method for the compressible Euler equations.*

(iv) *The simple splitting method we have described here is first order in time. Second order Strang splitting can be implemented similarly.*

3.1.4. The hybrid method (HM). The standard HM is based on the hybrid representation (28). In the DVM case we consider the hybrid representation for the function $f_{\mathcal{K}}$ instead of f using $\mathcal{E}_{\mathcal{K}}$ instead of $M_{f_{\mathcal{K}}}$. We have two differences with respect to (28): the function $f_{\mathcal{K}}$ and $\mathcal{E}_{\mathcal{K}}$ are piecewise constant and defined on a compact support (see Figure 2 for the representation of $\mathcal{E}(v)$ with respect to $M_f(v)$ in the continuous case). Thus we assume that the solution of the relaxation step has the form

$$f^r_k(x,t) = (1 - \beta^r(x,t)) f^{r,p}_k(x,t) + \beta^r(x,t)\mathcal{E}^r_k(x,t) \qquad \forall k \in K. \tag{60}$$

From the exact solution of the relaxation step (51) and the initial data, we could obtain the evolution of the unknowns $f^p_{k,i}$ and β^r_i; for the details of the computations we refer the reader to [13]:

$$f^{r,p}_k(x,t) = f^p_k(x, t=0) \qquad \forall k \in K, \tag{61}$$

$$\beta^r(x,t) = e^{-t/\varepsilon}\beta(x, t=0) + 1 - e^{-t/\varepsilon}. \tag{62}$$

Note that $\mathcal{E}^r_k(x,t) = \mathcal{E}_k(x, t=0)$ and that $\beta^r(x,t) \to 1$ as $\varepsilon \to 0$. If we start from $\beta(x, t=0) = 0$ (all particles) at the end of the relaxation, a fraction $1 - e^{-t/\varepsilon}$ of the particles is discarded by the method as the effect of the relaxation to equilibrium. Thus particles will represent the fractions $(1-\beta^r(x,t)) f^{r,p}_k(x,t)$. Moreover, the hybrid representation is naturally kept by the relaxation.

After relaxation the exact solution of the transport step reads

$$\begin{aligned} f^c_k(x,t) &= (1 - \beta^c(x,t)) f^{c,p}_k + \beta^c(x,t)\mathcal{E}^c_k(x,t) = f^r_k(x - v_k t, t) \\ &= (1 - \beta^r(x - v_k t, t)) f^{r,p}_k(x - v_k t, t) \\ &\quad + \beta^r(x - v_k t, t)\mathcal{E}^r_k(x - v_k t, 0) \qquad \forall k \in K. \end{aligned} \tag{63}$$

To simplify notation let us set

$$f_k^{*,p}(x,t) = (1-\beta^r(x-v_kt,t))f_k^{r,p}(x-v_kt,t) \qquad \forall k \in K,$$
$$\mathcal{E}_k^*(x,t) = \beta^r(x-v_kt,t)\mathcal{E}_k^r(x-v_kt,0) \qquad \forall k \in K.$$

Unfortunately now the hybrid structure of the solution is not kept since $\mathcal{E}_k^*(x,t)$ are not equilibrium states. For example the above set of equations can be solved taking

$$\beta^c(x,t) = 0 \tag{64}$$

and

$$f_k^{c,p}(x,t) = f_k^{*,p}(x,t) + \mathcal{E}_k^*(x,t) \qquad \forall k \in K. \tag{65}$$

The choice (64) means we completely lose, after the transport, the structure equilibrium/nonequilibrium. However, note that we do not need to resample the whole deterministic fraction; in fact, if we move one step t_1 further in the relaxation using $f_k^c(x,t)$ defined above as initial data, we have $\beta^r(x,t+t_1) = 1-e^{-t_1/\varepsilon}$ and

$$f_k^r(x,t+t_1) = e^{-t_1/\varepsilon}(f_k^{*,p} + \mathcal{E}_k^*(x,t)) + (1-e^{-t_1/\varepsilon})\mathcal{E}_k^r(x,t+t_1) \qquad \forall k \in K, \tag{66}$$

where $\mathcal{E}_k^r(x,t+t_1) = \mathcal{E}_k^c(x,t)$. Thus, in practice, we can avoid resampling particles after the convection and apply the resampling only on a fraction $e^{-t_1/\varepsilon}$ of the deterministic fraction as needed by the relaxation. More precisely, taking cell averages of (66) as in a standard Monte Carlo method, and using equations (56) for the reconstruction as shown later, the algorithm to compute the particles that represent the fractions $e^{-t_1/\varepsilon}f_k^c(x,t)$ in each interval reads as follows.

ALGORITHM 3 (hybrid Monte Carlo for DVM-BGK).

1. *Given* $m = \frac{\Delta x \triangle v}{N}\sum_i\sum_k f_{k,i}^c(t) = m^0 = \frac{\Delta x \triangle v}{N^0}\sum_i\sum_k f_{k,i}(t=0)$, *do the following:*
2. *For each interval* I_i, $i = \dots,-2,-1,0,1,2,\dots,$
   (a) *set* $\beta_i = 1-e^{-t_1/\varepsilon}$;
   (b) *set* $N_i = \text{Iround}\left((1-\beta_i)\frac{\Delta x \triangle v}{m}\sum_k f_{k,i}^c(t)\right)$;
   (c) *set* $P_i = \frac{u_{p,i}^*(t)}{u_{p,i}^*(t)+u_{\mathcal{E},i}^*(t)}$,
   with $u_{p,i}^*(t) = \sum_k f_{k,i}^{*,p}(t)$
   and $u_{\mathcal{E},i}^*(t) = \sum_k \mathcal{E}_{k,i}^*(t)$;
   (d) *for* $k = 1,\dots,N_i$
   with probability P_i *take* (ν_j,χ_j) *as one of the advected particles;*
   with probability $1-P_i$ *take one sample* ν_j *from the deterministic fraction.*
   To extract $(1-P_i)N_i$ *samples from a discrete advected Maxwellian do the following:*
      i. *Compute* $p_{k,i} = \frac{\mathcal{E}_{k,i}^*\cdot\Delta v}{\varrho_i}$.
      ii. *Compute* $P_{k,i} = \sum_{\mathcal{K}} p_{k,i}$, $k = 1,..,K$, $P_{0,i} = 0$.
      iii. *Compute a random number* ξ.
      iv. *Find the integer* k *such that* $P_{k-1,i} \le \xi < P_{k,i}$.
      v. *Give to the sample* ν_j *the velocity* v_{k-1}.

After this the hybrid solution is computed simply by adding the deterministic terms

$$\beta_i\mathcal{E}_{k,i}^r(t+t_1) \qquad \forall k \in K$$

to the stochastic terms

$$(1-\beta_i) f_{k,i}^{r,p}(t+t_1) \qquad \forall k \in K.$$

Note that as $\varepsilon \to 0$ we do not perform any resampling at all, and we obtain a relaxation scheme for the limiting Euler equations. We denote with the shorthand HM the hybrid scheme based on the above algorithm to determine the fraction of solution represented by particles which make use of the choice (64) after the transport.

REMARK 3.

(i) *The convection part corresponding to $f_k^{*,p}(x,t)$ is solved exactly by transport of particles as in a full Monte Carlo method. At variance the convection part corresponding to $\mathcal{E}_k^*(x,t)$ is solved by a finite volume scheme for a DVM.*

(ii) *Note that the effective value of β_i used in the above algorithm differs from $1-e^{-t_1/\varepsilon}$. In fact if N_i^c denotes the number of particles in cell i after the convection step, during the relaxation we keep only an integer approximation N_i^β of $(1-\beta_i)N_i^c$. The effective value of β_i can then be computed at the end of the algorithm as*

$$\beta_i^E = 1 - \frac{N_i^\beta}{N_i^c}.$$

3.1.5. Componentwise hybrid method (CHM). Another approach consists in finding the maximum value of $\beta^c(x,t) > 0$ in order to maximize the deterministic fraction in equations (63). To achieve this goal we start from representation (24), which gives for the relaxation step

$$f_k^r(x,t) = \tilde{f}_k^r(x,t) + w_k^r(x,t)\mathcal{E}_k^r(x,t) \qquad \forall k \in K. \tag{67}$$

The evolution for the unknowns $\tilde{f}_k^r(x,t)$, $w_k^r(x,t)$ are now (see [13] for details)

$$\tilde{f}_k^r(x,t) = e^{-t/\varepsilon}\tilde{f}_k(x,t=0), \quad w_k^r(x,t) = e^{-t/\varepsilon}w_k(x,t=0)+1-e^{-t/\varepsilon} \quad \forall k \in K. \tag{68}$$

As before the hybrid representation is kept by the relaxation process. The only difference with respect to the HM is that particles are discarded from f_k with different ratios, depending on the local equilibrium degree.

Again the convection destroys the structure of the solution, and we get

$$\begin{aligned} f_k^c(x,t) &= \tilde{f}_k^c(x,t) + w_k^c(x,t)\mathcal{E}_k^c(x,t) = f_k^r(x-v_kt,t) \\ &= \tilde{f}_k^r(x-v_kt,t) + w_k^r(x-v_kt,t)\mathcal{E}_k^r(x-v_kt,0) \qquad \forall k \in K. \end{aligned} \tag{69}$$

To simplify notation let us set

$$f_k^{*,p}(x,t) = \tilde{f}_k^r(x-v_kt,t), \quad \tilde{\mathcal{E}}_k(x,t) = w_k^r(x-v_kt,t)\mathcal{E}_k^r(x-v_kt,0) \quad \forall k \in K.$$

Here we do not assume $w_k^c(x,t) = 0\ \forall k \in K$, since we want to take advantage of the componentwise hybrid representation in order to maximize the deterministic fraction of the solution. Thus, starting from the deterministic fractions $\tilde{\mathcal{E}}_k(x,t)$ defined above we construct the new values of $w_k^c(x,t)$, $\tilde{f}_k^c(x,t)$, using Definition 1 in the case of piecewise constant functions defined on a compact support.

More precisely, we define

$$w_k^c(x,t) = \begin{cases} \dfrac{\tilde{\mathcal{E}}_k(x,t)}{\mathcal{E}_k^c(x,t)}, & \tilde{\mathcal{E}}_k(x,t) \le \mathcal{E}_k^c(x,t) \neq 0 \\ 1, & \tilde{\mathcal{E}}_k(x,t) > \mathcal{E}_k^c(x,t) \end{cases} \qquad \forall k \in K \tag{70}$$

and

$$\mathcal{E}_k^*(x,t) = \tilde{\mathcal{E}}_k(x,t) - w_k^c(x,t)\mathcal{E}_k^c(x,t) \qquad \forall k \in K. \tag{71}$$

In this way we obtain

$$\tilde{f}_k^c(x,t) = f_k^{*,p}(x,t) + \mathcal{E}_k^*(x,t) \qquad \forall k \in K. \tag{72}$$

The HM based on the computations of the equilibrium fraction after the transport through (70) will be called CHM. The next relaxation step then applies as in the HM case, substituting the value $\tilde{f}_k^c(x,t)$ with the relation above:

$$\begin{aligned} f_k^r(x,t+t_1) &= \tilde{f}_k^r(x,t+t_1) + w_k^r(x,t+t_1)\mathcal{E}_k^r(x,t+t_1) \\ &= e^{-t_1/\varepsilon} f_k^c(x,t) + (1-e^{-t_1/\varepsilon})\mathcal{E}_k^c(x,t) \\ &= e^{-t_1/\varepsilon}(f_k^{*,p}(x,t) + \mathcal{E}_k^*(x,t) + w_k^c(x,t)\mathcal{E}_k(x,t)) \\ &\quad + (1-e^{-t_1/\varepsilon})\mathcal{E}_k(x,t) \qquad \forall k \in K. \end{aligned} \tag{73}$$

If we define after the convection step

$$\beta^c(x,t) = \min\{w_k^c(x,t)\} \qquad \forall k \in K, \tag{74}$$

we maximize the common value of β^c such that the standard HM applies; that particular choice leads to another hybrid scheme that will be called HMI. This could be very relevant in applications where it is important that the hybrid decomposition is component independent. For instance if we want to treat the equilibrium part through a macroscopic scheme, we have to adopt this strategy. The independent fluid solver strategy will be the subject of a future work [15].

3.2. Hybrid Boltzmann–BGK schemes. The use of a DVM presents several drawbacks. First, since the discrete local Maxwellian equilibrium is needed explicitly, we need a suitable numerical method to solve the nonlinear system of equations (41). From the computational side this leads to an increase of computational cost, which is especially relevant in higher dimensions. Next, since discrete Maxwellian equilibrium states are compactly supported they differ from Maxwellians of the Boltzmann equation. Thus the corresponding fluid equations may be different from the classical ones (see Figures 2 and 3); in other words a DVM cannot describe correctly all possible flows [26]. For this reason it is highly desirable to have a method which is not based on the use of a DVM.

The idea is to split the Maxwellian into two parts:

$$M(v) = E_R(v) + T_R(v), \tag{75}$$

where $E_R(v) = M(v)\Psi(|v| \le R)$, $R > 0$, represents the central part of the solution and $T_R(v) = M(v)\Psi(|v| > R)$ the tails. The starting point of such schemes is given by representations (31) and (35).

Since the schemes follow the same lines of the ones described for the DVM-BGK model, we will describe them briefly by emphasizing only the major differences.

3.2.1. Boltzmann hybrid method (BHM). We start by again splitting our problem into relaxation and transport steps and using representation (35). The solution of the relaxation now reads

$$f_R^r(x,v,t) = \left(1 - \frac{\rho_E^r(x,t)}{\rho^r(x,t)}\beta_R^r(x,t)\right) f_R^{r,p}(x,v,t) + \beta_R^r(x,t)E_R^r(x,v,t), \tag{76}$$

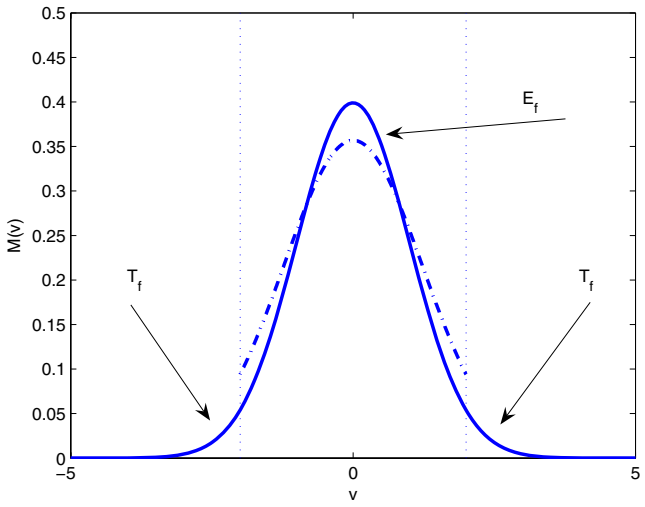

FIG. 2. *Discrete Maxwellian on a truncated velocity domain (dashed lines) and corresponding Maxwellian with the same mass, momentum, and energy.*

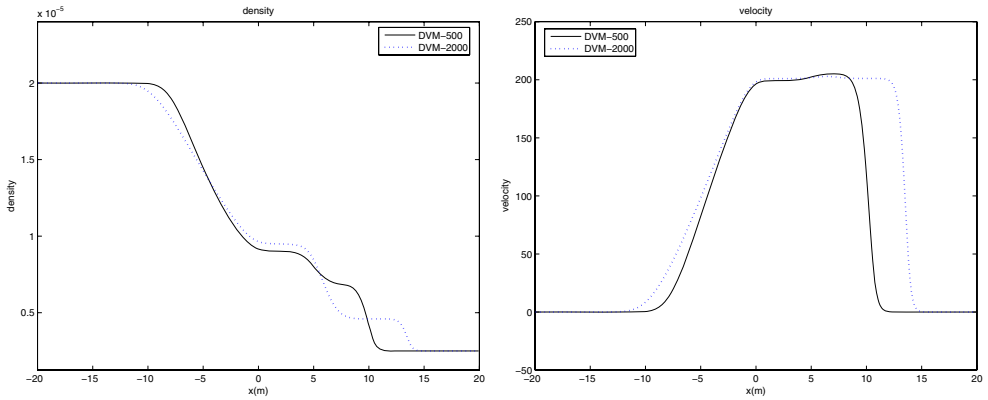

FIG. 3. *Density (left) and velocity (right) profiles for the Sod test with initial data* $\varrho_L = 2\times10^{-5}$, $u_L = 0$, $T_L = 273.15$ *and* $\varrho_R = 0.25 \times 10^{-5}$, $u_R = 0$, $T_R = 273.15$. *The limit* $\varepsilon \to 0$ *for DVM schemes with velocity range* $[-2000, 2000]$ *and* $[-500, 500]$, *respectively.*

where

$$\rho^r(x,t) = \int f_R^r(x,v,t)dv = \int f_R^{r,p}(x,v,t)dv.$$

As before, using the exact solution of the relaxation step starting from initial data at $t = 0$ we are able to compute the evolution equations for the unknowns $f_R^{r,p}(x,t)$ and $\beta_R^r(x,t)$. The equation for $\beta_R^r(x,t)$ is the same as in scheme HM:

$$\beta_R^r(x,t) = e^{-t/\varepsilon}\beta_R(x,0) + 1 - e^{-t/\varepsilon}, \tag{77}$$

whereas the equation for the particle distribution now takes into account the changes due to the presence of the tails:

$$f_R^{r,p}(x,v,t) = \frac{e^{-t/\varepsilon}\beta_R(x,0) + 1 - e^{-t/\varepsilon}}{a-b} T_R(x,v,0) + \frac{1}{a-b}\left(e^{-t/\varepsilon}\left(1 - \frac{\rho_E(x,0)}{\rho(x,0)}\beta_R(x,0)\right)\right) f_R^p(x,v,0), \tag{78}$$

where

$$b = (1-e^{-t/\varepsilon})\left(\frac{\rho_E(x,0)}{\rho(x,0)}\right), \qquad a = \left(1 - \frac{\rho_E(x,0)}{\rho(x,0)}\beta_R(x,0)e^{-t/\varepsilon}\right).$$

The major difference is that as $\varepsilon \to 0$ a fraction $(1-\rho_E^r(x,t)/\rho^r(x,t))$ of the solution is still represented by particles. After relaxation we transport the particles and the equilibrium part as before to obtain

$$\begin{aligned} f_R^c(x,v,t) &= \left(1 - \frac{\rho_E^c(x,t)}{\rho^c(x,t)}\beta_R^c(x,t)\right) f_R^{c,p}(x,v,t) + \beta_R^c(x,t) E_R^c(x,v,t) \\ &= f_R^{*,p}(x,v,t) + E_R^*(x,v,t). \end{aligned} \tag{79}$$

Finally, we reproject the solution into the form (35) by taking $\beta_R^c = 0$ as in scheme HM.

The treatment of the nonequilibrium part of the solution has been done using a discrete velocity Monte Carlo scheme for the central part and a general Monte Carlo scheme (i.e., samples can attain any velocity) for the tails. The details of the Boltzmann hybrid method are given in the following algorithm.

ALGORITHM 4 (BHM scheme).

1. *Given* $m = \frac{\Delta x}{N}\sum_i \varrho_{i,R}^c(t)$, *where* $\varrho_{i,R}^c(t)$ *represent the total mass in each cell at time* t *after convection, which now differs from* $\triangle v \sum_k f_{k,i,R}^c(t)$, *do the following:*
2. *For each interval* I_i, $i = \dots, -2, -1, 0, 1, 2, \dots$,
   (a) *set* $\beta_i = 1 - e^{-t_1/\varepsilon}$;
   (b) *set* $N_i = \text{Iround}\left((1-\beta_i)\frac{\Delta x}{m}\varrho_i^c(t)\right)$;
   (c) *set* $P_i = \frac{u_{p,i}^*(t)}{u_{p,i}^*(t)+u_{E,i}^*(t)}$,
   with $u_{p,i}^*(t) = \frac{m}{\Delta x}\sum_{\chi_k \in I_i} 1 = \frac{m}{\Delta x}N_j$, *where* N_j *indicate the particles that belong to the cell* I_i
   and $u_{E,i}^*(t) = \sum_k E_{k,i,R}^*(t)$;
   (d) *for* $k = 1, \dots, N_i$
   with probability P_i *take* (ν_j, χ_j) *as one of the advected particles;*
   with probability $1-P_i$ *take one sample* ν_j *from the deterministic fraction. To extract* $(1-P_i)N_i$ *samples from the discrete advected central part of the Maxwellian do the following:*
      i. *Compute* $p_{k,i} = \frac{E_{k,i,R}^* \cdot \Delta v}{\varrho_i}$.
      ii. *Compute* $P_{k,i} = \sum_{\mathcal{K}} p_{k,i}$, $k = 1, .., K$, $P_{0,i} = 0$.
      iii. *Compute a random number* ξ.
      iv. *Find the integer* k *such that* $P_{k-1,i} \le \xi < P_{k,i}$.
      v. *Give to the sample* ν_j *the velocity* v_{k-1}.
   (e) *Set* $N_i^T = \text{Iround}\left(\beta_i\left(\frac{\Delta x}{m}\varrho_{i,R}^c(t) - \frac{\Delta x \triangle v}{m}\sum_k f_{k,i,R}^c(t)\right)\right)$.
   (f) *For* $k = 1, .., N_i^T$ *extract a sample from the tail of the Maxwellian. To extract a sample from the right tail do the following:*
      i. *Compute* $r = \cos(2 * \pi * \xi_1)$.

ii. *If* $r > 0$, *compute* $v = \sqrt{-\log(\exp(-R^2) - \xi_2 * \exp(-R^2))}$ *with* ξ_1, ξ_2 *random numbers in* $[0,1]$.
iii. *If* $v > R$, *take the sample; else reject the sample.*

As for the HM scheme the final solution is recovered by adding the deterministic term $\beta_i\, E_{k,i,R}(t)$ to the stochastic term.

3.2.2. Boltzmann componentwise hybrid method (BCHM). The componentwise approach described in the previous section can be adapted to the case of representation (31). We have

$$f^r(x,v,t) = \tilde{f}^r_R(x,v,t) + w^r_R(x,v,t) M^r(x,v,t). \tag{80}$$

The evolutions for the unknowns $\tilde{f}^r_R(x,v,t)$, $w^r_R(x,v,t)$ are now

$$\tilde{f}^r_R(x,v,t) = e^{-t/\varepsilon} \tilde{f}_R(x,v,0) + (1 - e^{-t/\varepsilon}) T_R(x,v,0), \tag{81}$$

$$w^r_R(x,v,t) = e^{-t/\varepsilon} w_R(x,v,0) + (1 - e^{-t/\varepsilon}) \Psi(|v| \le R). \tag{82}$$

Clearly, as in scheme BHM, as $\varepsilon \to 0$ a fraction of the solution is represented by particles. Again after convection we have

$$f^c_R(x,v,t) = \tilde{f}^c(x,v,t) + w^c_R(x,v,t) M^c(x,v,t) = f^{*,p}_R(x,v,t) + \tilde{M}^r(x,v,t),$$

where $f^{*,p}_R(x,v,t)$ and $\tilde{M}^r(x,v,t)$ represent the advected particles and equilibrium fractions. The value $w^c_R(x,v,t)$ is now computed only in the central part of f, $|v| \le R$, by

$$w^c_R(x,v,t) = \begin{cases} \dfrac{\tilde{M}^r(x,v,t)}{M^c(x,v,t)}, & \tilde{M}^r(x,v,t) \le M^c(x,v,t) \ne 0, \\ 1, & \tilde{M}^r(x,v,t) > M^c(x,v,t). \end{cases} \tag{83}$$

Then we define

$$M^*(x,v,t) = \tilde{M}^r(x,v,t) - w^c_R(x,v,t) M^c(x,v,t)$$

to obtain

$$\tilde{f}^c(x,v,t) = f^{*,p}_R(x,v,t) + M^*(x,v,t). \tag{84}$$

Finally, the same strategy, described in the previous section, of taking $\beta^c_R(x,t) = \min_v\{w^c_R(x,v,t)\}$ could be adopted for applications in which the decomposition is component independent. We omit the details.

4. Numerical tests. In this section we compare the performance of the Monte Carlo and the hybrid schemes presented here using two classical tests: a Sod test and an unsteady shock test. We have chosen two unsteady tests because we would like to test the performance of the methods without the effect of averaging the solution in time (typical of Monte Carlo methods for steady problems). Before this, however, we have performed an overall accuracy test of the different schemes.

4.1. Accuracy test. We report the total L_1 norm of the errors for the conserved quantities ϱ, u, and T by considering a periodic smooth solution with initial data

$$\begin{aligned} \varrho(x,0) &= 1 + a_\varrho \sin\frac{2\pi x}{L}, \\ u(x,0) &= 1 + a_u \sin\frac{2\pi x}{L}, \\ T(x,0) &= 1 + a_T \sin\frac{2\pi x}{L}, \end{aligned} \tag{85}$$

TABLE 1
Accuracy test, L_1 norm of the errors for density with respect to different values of the Knudsen number ε (in units of 10^{-2}).

	$\varepsilon = 10^{-2}$	$\varepsilon = 10^{-3}$	$\varepsilon = 10^{-4}$	$\varepsilon = 10^{-5}$	$\varepsilon = 10^{-6}$
MCM	2.1512	2.3435	2.6886	2.6684	2.6529
HM	2.0234	1.7406	1.2126	0.4020	0.12868
HMI	1.9934	1.600	0.7888	0.2895	0.0961
CHM	1.1704	0.6233	0.2743	0.10938	0.0309
BHM	1.9660	1.9125	1.3499	0.8163	0.7258
BHMI	1.7115	1.4536	0.7517	0.7212	0.6866
BCHM	1.4685	0.9204	0.7000	0.6439	0.6538

TABLE 2
Accuracy test, L_1 norm of the errors for velocity with respect to different values of the Knudsen number ε (in units of 10^{-2}).

	$\varepsilon = 10^{-2}$	$\varepsilon = 10^{-3}$	$\varepsilon = 10^{-4}$	$\varepsilon = 10^{-5}$	$\varepsilon = 10^{-6}$
MCM	2.9320	3.5061	4.8096	4.626	4.6652
HM	2.8686	2.2685	2.1736	0.7182	0.2503
HMI	2.3551	1.9552	1.3733	0.4994	0.1851
CHM	1.3448	0.9139	0.4739	0.1662	0.0527
BHM	3.0944	2.5336	2.4123	1.5215	1.2635
BHMI	2.5098	2.2245	1.4186	1.4417	1.3714
BCHM	1.8727	1.5825	1.4079	1.2246	1.2355

TABLE 3
Accuracy test, L_1 norm of the errors for temperature with respect to different values of the Knudsen number ε (in units of 10^{-2}).

	$\varepsilon = 10^{-2}$	$\varepsilon = 10^{-3}$	$\varepsilon = 10^{-4}$	$\varepsilon = 10^{-5}$	$\varepsilon = 10^{-6}$
MCM	3.2923	4.4354	6.2404	5.7733	6.1142
HM	2.9520	2.7893	2.6305	0.96996	0.2840
HMI	2.8437	2.5110	1.6132	0.6617	0.2053
CHM	1.8196	1.2004	0.5368	0.1310	0.0651
BHM	3.1869	3.0254	2.8536	2.1430	1.8134
BHMI	2.7132	2.6807	2.3756	2.0148	2.1010
BCHM	2.6210	2.3226	2.1498	1.9315	1.8849

where we set

$$a_\varrho = 0.3, \quad a_u = 0.1, \quad a_T = 1.$$

We use 1500 particles for cell with bounds set at $[-15, 15]$ for the DVM-BGK schemes and bounds set at $[-5, 5]$ for the Boltzmann–BGK schemes; we integrate the equations for $t \in [0, 5 \times 10^{-2}]$ for $\Delta v = 0.16$ and $\Delta x = 0.05$. We compare our hybrid solutions with a reference solution obtained with a fully deterministic DVM-BGK model with the same Δv and Δx but with bounds set at $[-20, 20]$ in velocity space.

We use the shorthand MCM, HM, HMI, CHM, BHM, BHMI, BCHM to denote the Monte Carlo scheme, the DVM–BGK hybrid schemes (respectively, (64), (74), (70)), and the Boltzmann–BGK hybrid schemes with the same choice of $\beta^c(x, t)$. The results for the relative L_1 errors are reported in Tables 1, 2, and 3. The parameters that influence the numerical solution in all the schemes are the number of particles and the number of mesh points in velocity space. Moreover, DVM-BGK schemes are influenced by the truncation of the velocity space and by the method we use to solve the nonlinear system (41), while BHM schemes are influenced by the position of the

TABLE 4
Computational time test for different values of the Knudsen number ε.

	$\varepsilon = 10^{-2}$	$\varepsilon = 10^{-3}$	$\varepsilon = 10^{-4}$	$\varepsilon = 10^{-5}$	$\varepsilon = 10^{-6}$
MCM	23 sec	25 sec	27 sec	26 sec	27 sec
BHM	35 sec	25 sec	22 sec	22 sec	21 sec
BHMI	34 sec	20 sec	19 sec	20 sec	21 sec
BCHM	15 sec	11 sec	17 sec	21 sec	20 sec

boundary that divides E_f from T_f, which turns in a different number of particles in the domain. The schemes HM, HMI, and CHM cause a progressive reduction of fluctuations as the Knudsen number decreases. On the other hand, the deterministic computation of the function $\mathcal{E}$ and of the large velocity components is expensive, and the hybrid schemes, independently of ε, are computationally more expensive than MCM.

The Boltzmann–BGK solvers are faster since we do not need to compute the solution of a nonlinear system at each time step for each component of $\mathcal{E}$. They are also faster because the deterministic solvers contain fewer mesh points. However, BHM, BHMI, and BCHM present more fluctuations with respect to HM, HMI, and CHM because tails are represented by particles. We report the corresponding computational times for the Boltzmann–BGK schemes with respect to the MCM scheme for different Knudsen numbers in Table 4. Note that all these schemes are more accurate and more efficient than MCM. In particular BCHM for $\varepsilon = 10^{-3}$ is about twice as fast and twice as accurate as MCM.

We remark that no attempt to optimize the truncation parameter in the Boltzmann–BGK schemes has been made in order to obtain the optimum compromise between accuracy and computational time.

4.2. Sod test. We consider the classical Sod test with initial value

$$\text{(86)}\quad \begin{pmatrix} \varrho_L \\ u_L \\ T_L \end{pmatrix} = \begin{pmatrix} 1 \\ 0 \\ 5 \end{pmatrix} \text{ if } 0 \leqq x < 0.5, \qquad \begin{pmatrix} \varrho_R \\ u_R \\ T_R \end{pmatrix} = \begin{pmatrix} 0.125 \\ 0 \\ 4 \end{pmatrix} \text{ if } 0.5 \leqq x \leqq 1.$$

The solution is computed with 200 space points in $[0, 1]$, and the final time is $t = 0.05$. The initial number of particles is 1000 for each space cell; the Knudsen number is $\varepsilon = 10^{-3}$ in one case and $\varepsilon = 10^{-5}$ in the other. In the HM, HMI, and CHM schemes the velocity space is bounded at $[-15, 15]$ and discretized with $\Delta v = 0.16$. The bounds between the tails and the central part of the Maxwellian for BHM, BHMI, and BCHM are set to $[-5, 5]$, with the same mesh in velocity. We compare our solutions with a reference solution obtained with a DVM model with 500 space cells and 250 cells in velocity space with bounds set at $[-20, 20]$ in velocity. From Figures 4, 5, 6, and 7 it is clear that all hybrid schemes provide a more accurate solution with fewer fluctuations with respect to MCM method.

4.3. Unsteady shock test. We consider an unsteady shock that propagates from left to right; the shock is produced introducing a specular wall in the left boundary, and this corresponds to putting an incoming Maxwellian distribution in the ghost cell with parameters ϱ, u, T equal to the parameters $\varrho(1)$, $u(1)$, $T(1)$ in the first cell. At the beginning the flow is uniform with

$$\text{(87)}\qquad \varrho(x, 0) = 1, \quad u(x, 0) = -1, \quad T(x, 0) = 4.$$

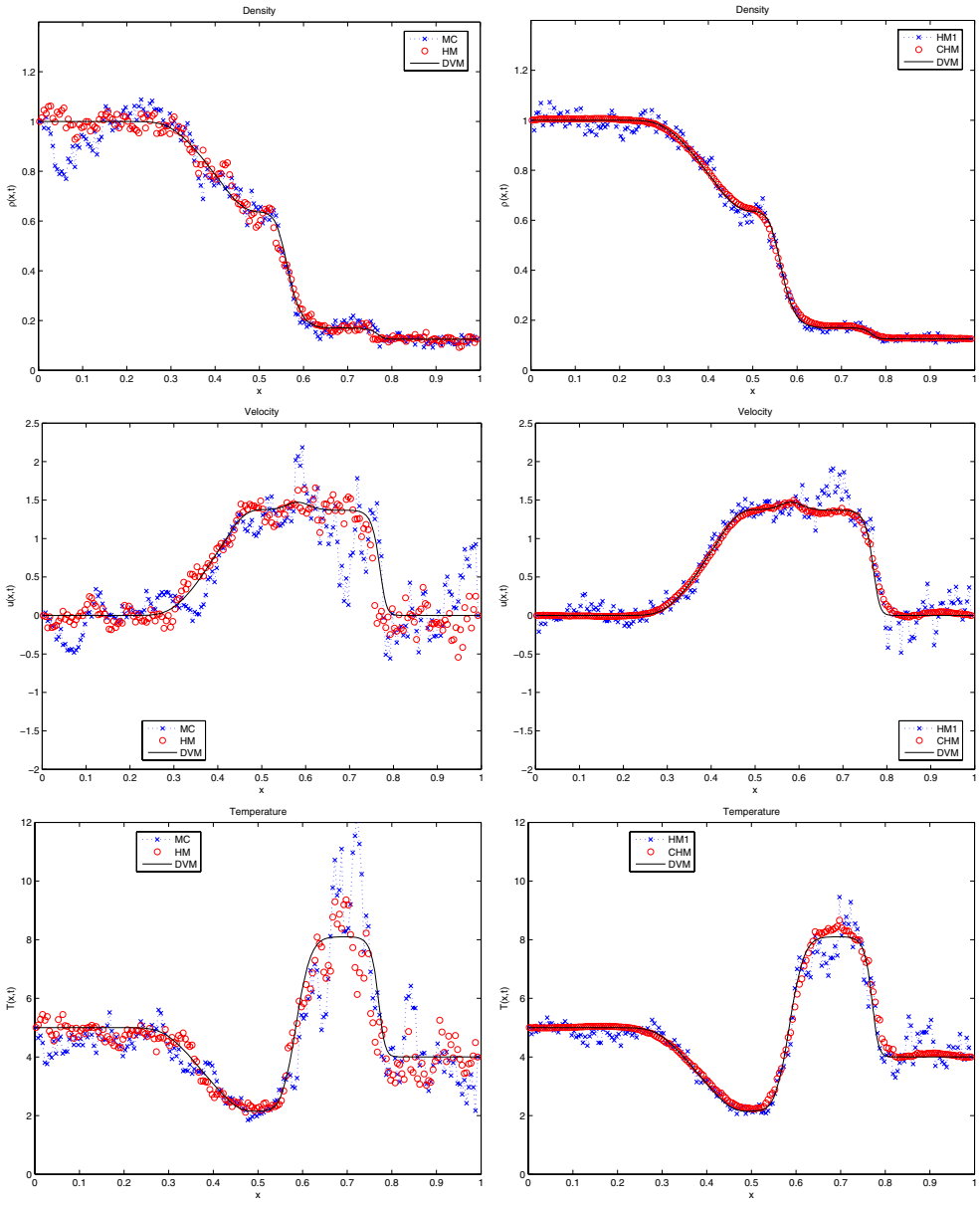

FIG. 4. *Sod test: Solution at* $t = 0.05$ *with* $\varepsilon = 10^{-3}$ *for density (top), mean velocity (middle), and temperature (bottom) for MCM and HM (left), HMI and CHM (right), with initial data* (86).

The computation is stopped when $t = 0.065$, the number of space cells is 200 in $[0, 1]$, the initial number of particles is 1500 for each space cell, and the Knudsen number is $\varepsilon = 10^{-3}$ in one case and $\varepsilon = 10^{-5}$ in the other. In the HM, HMI, and CHM schemes the velocity space is discretized with $\Delta v = 0.16$, and the bounds are set at $[-15, 15]$. The bounds between the tails and the central part of the Maxwellian for BHM, BHMI, and BCHM are set to $[-5, 5]$, with the same mesh in velocity. We again compare our solution with a DVM with 500 space cells and 250 cells in velocity space with bounds

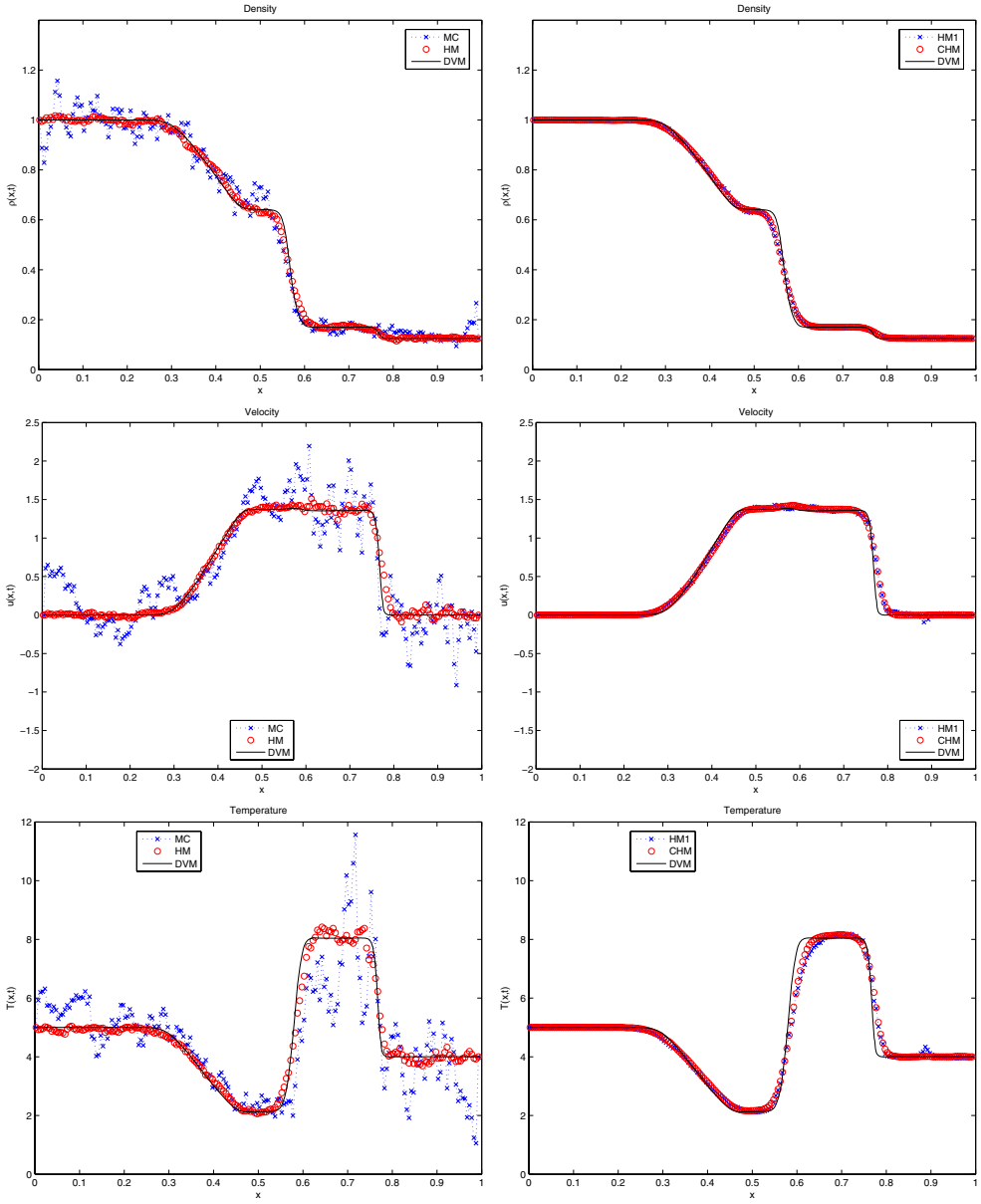

FIG. 5. *Sod test: Solution at* $t = 0.05$ *with* $\varepsilon = 10^{-5}$ *for density (top), mean velocity (middle), and temperature (bottom) for MCM and HM (left), HMI and CHM (right), with initial data* (86).

set at $[-20, 20]$. Again the improvement obtained with the hybrid schemes is clear (see Figures 8, 9, 10, and 11).

5. Conclusion. In this work we have considered the development of hybrid methods for kinetic multiscale problems. Although we have described the schemes in the case of Boltzmann–BGK equation, our approach can be extended to other kinetic equations. The additional difficulty usually is represented by the structure of the collision operator which requires a specific treatment (see [6, 28, 29] for the case

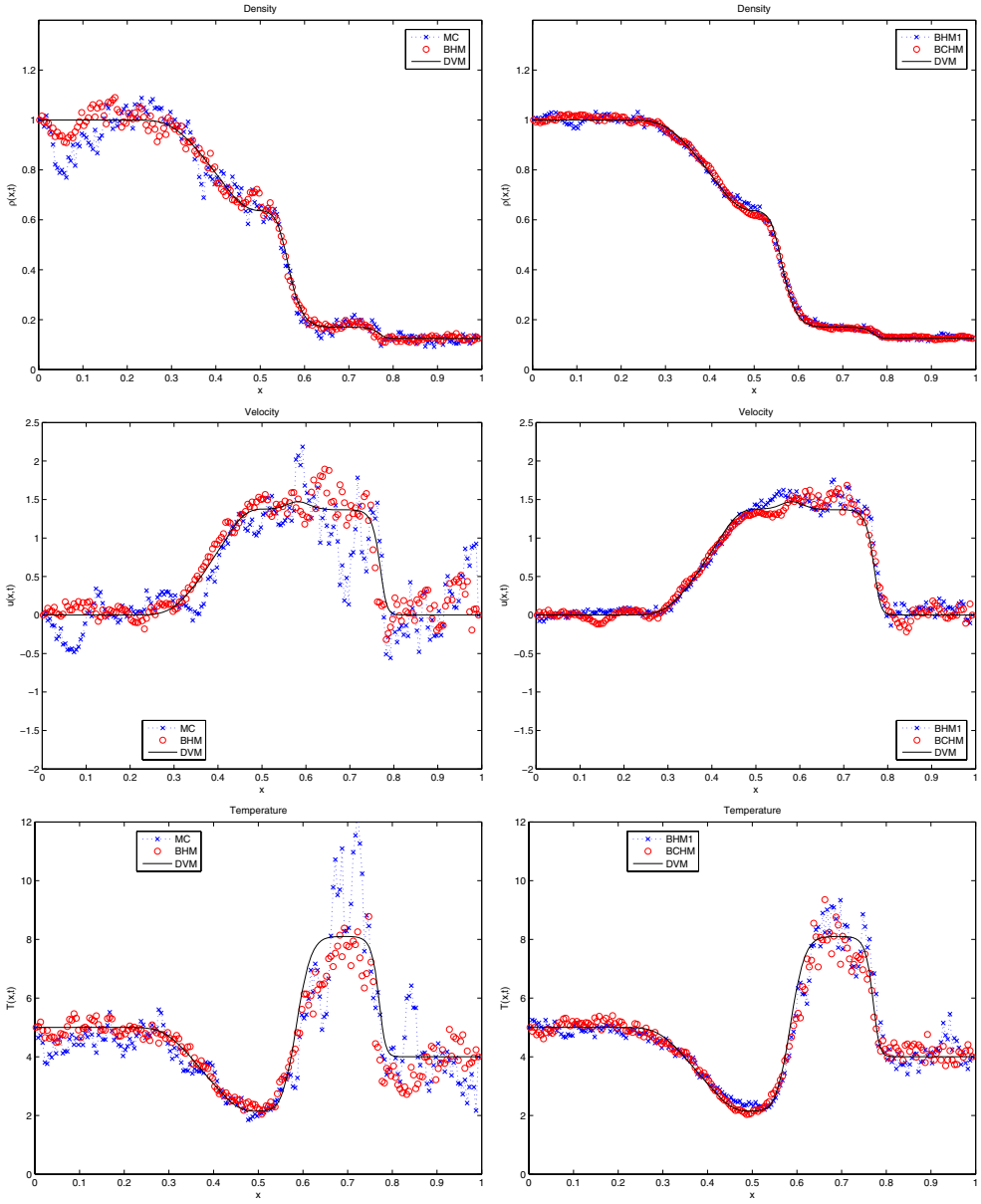

FIG. 6. *Sod test: Solution at* $t = 0.05$ *with* $\varepsilon = 10^{-3}$ *for density (top), mean velocity (middle), and temperature (bottom) for MCM and BHM (left), BHMI and BCHM (right), with initial data* (86).

of the full Boltzmann equation).

The hybrid multiscale methods developed here can be used in all cases where a macroscopic description of the phenomena is known but ceases to be valid in some region of the computational domain and the microscopic model has to be used. The necessary condition is that the microscopic variables and the macroscopic conserved variables are linked through an operator that define a local equilibrium.

The general approach consists in a suitable blending of deterministic methods

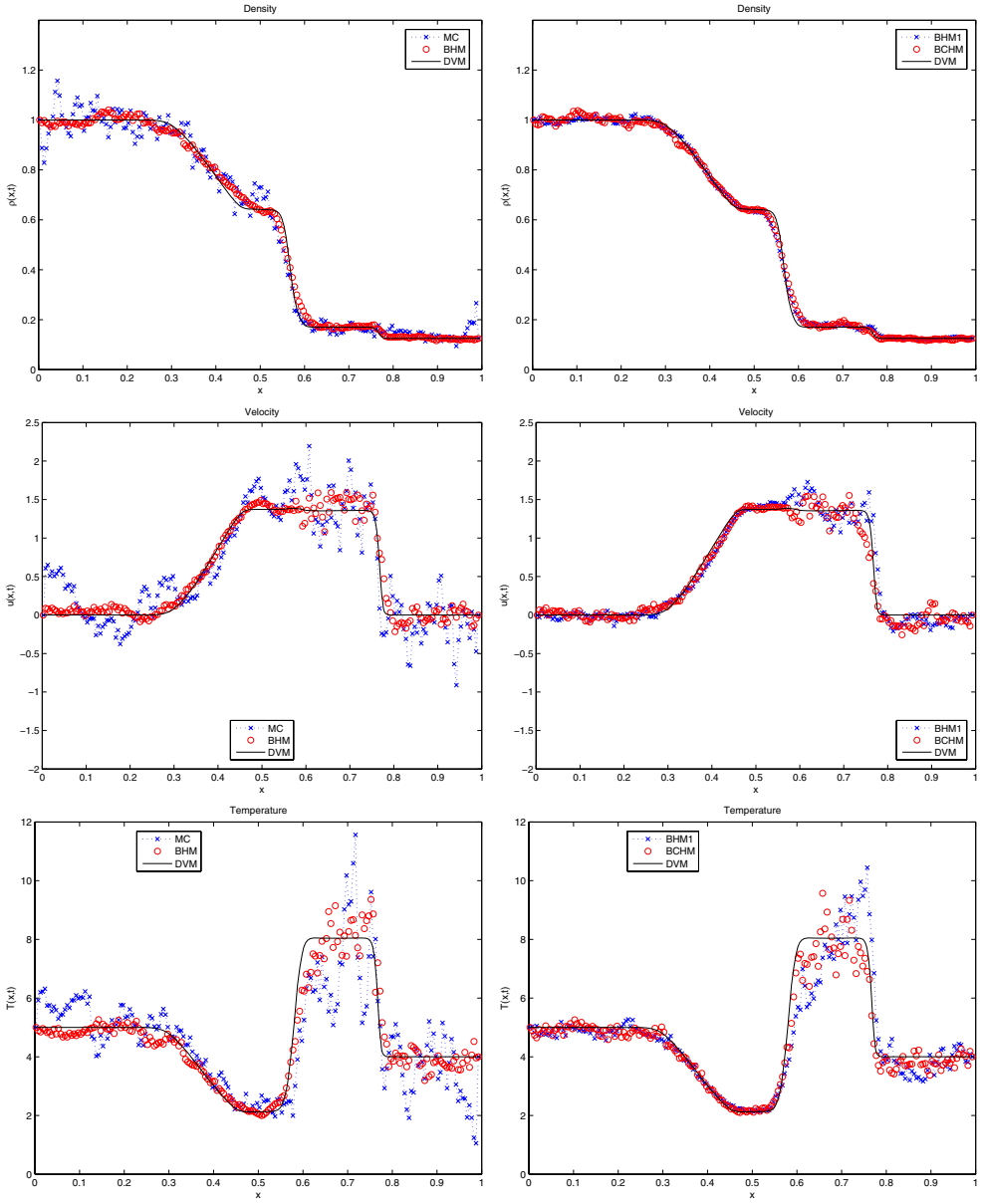

FIG. 7. *Sod test: Solution at* $t = 0.05$ *with* $\varepsilon = 10^{-5}$ *for density (top), mean velocity (middle), and temperature (bottom) for MCM and BHM (left), BHMI and BCHM (right), with initial data* (86).

for the equilibrium part and particle methods for the nonequilibrium part. Several numerical examples are shown in order to prove the validity and efficiency of the new methods. Of course other tests have to be done to measure the performance of the hybrid methods in real applications.

Acknowledgment. The authors would like to thank Russ Caflisch for the many stimulating discussions.

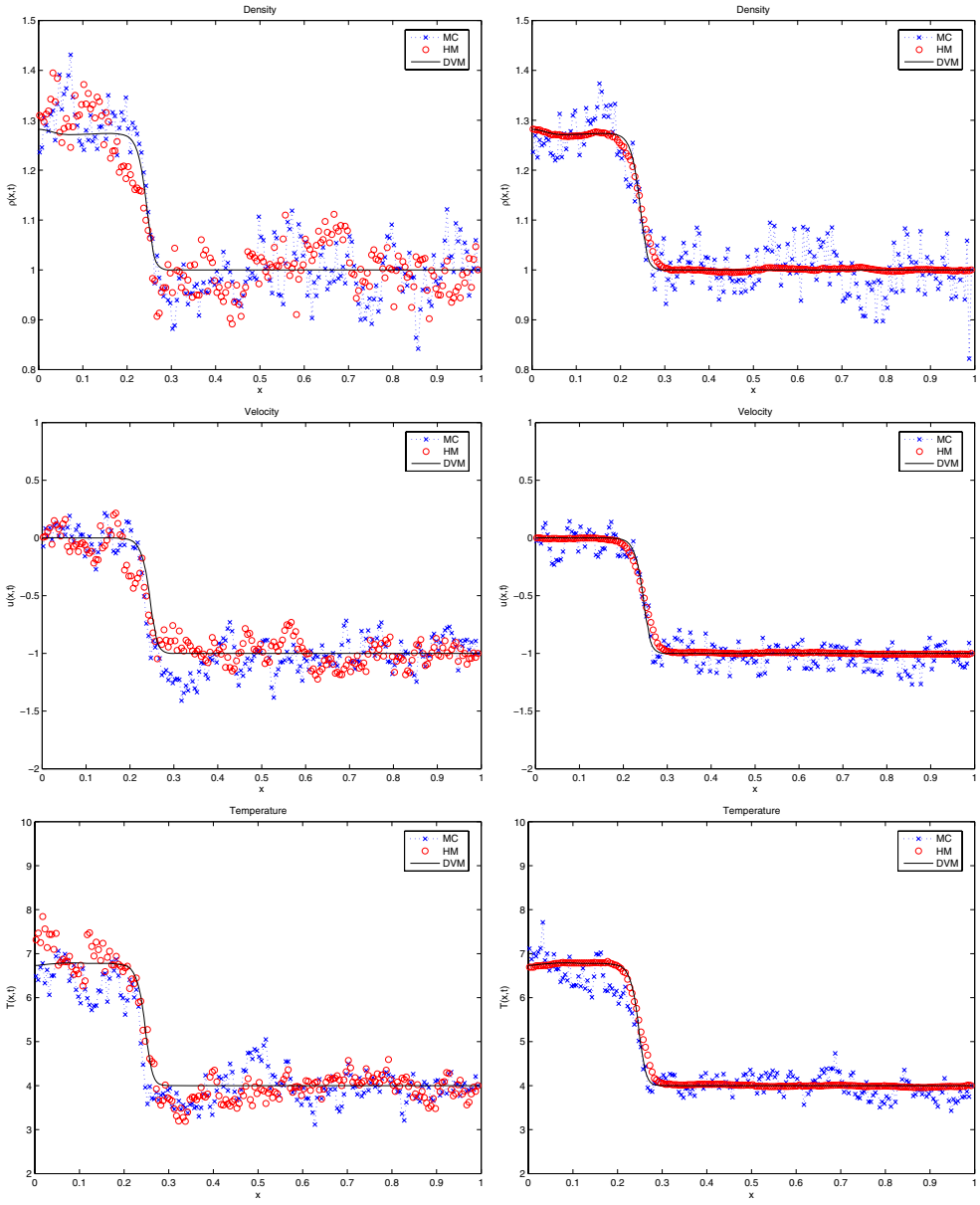

FIG. 8. *Unsteady shock: Solution at* $t = 0.065$ *with* $\varepsilon = 10^{-3}$ *for density (top), mean velocity (middle), and temperature (bottom) for MCM and HM (left), HMI and CHM (right), with initial data* (87).

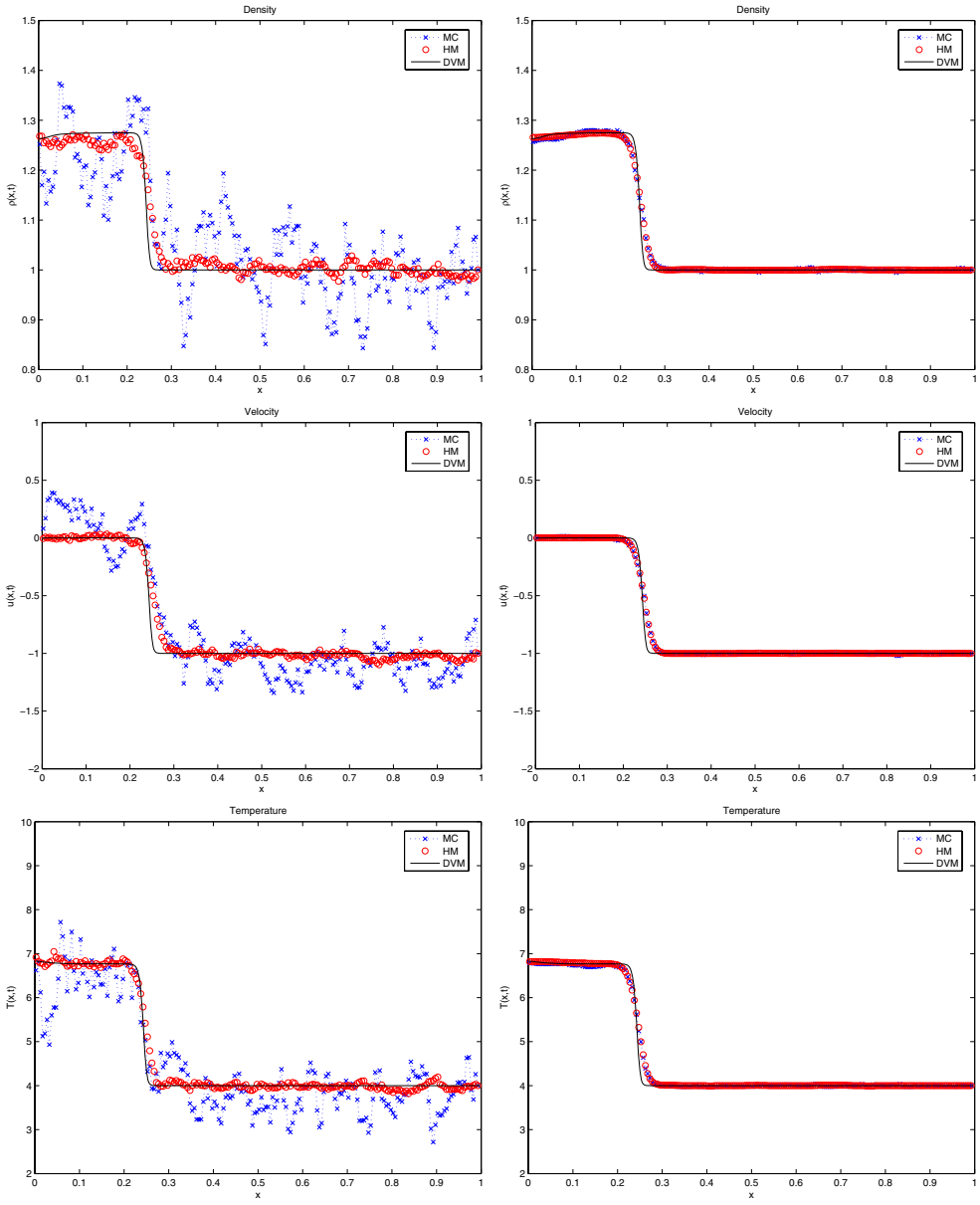

FIG. 9. *Unsteady shock: Solution at* $t = 0.065$ *with* $\varepsilon = 10^{-5}$ *for density (top), mean velocity (middle), and temperature (bottom) for MCM and HM (left), HMI and CHM (right), with initial data* (87).

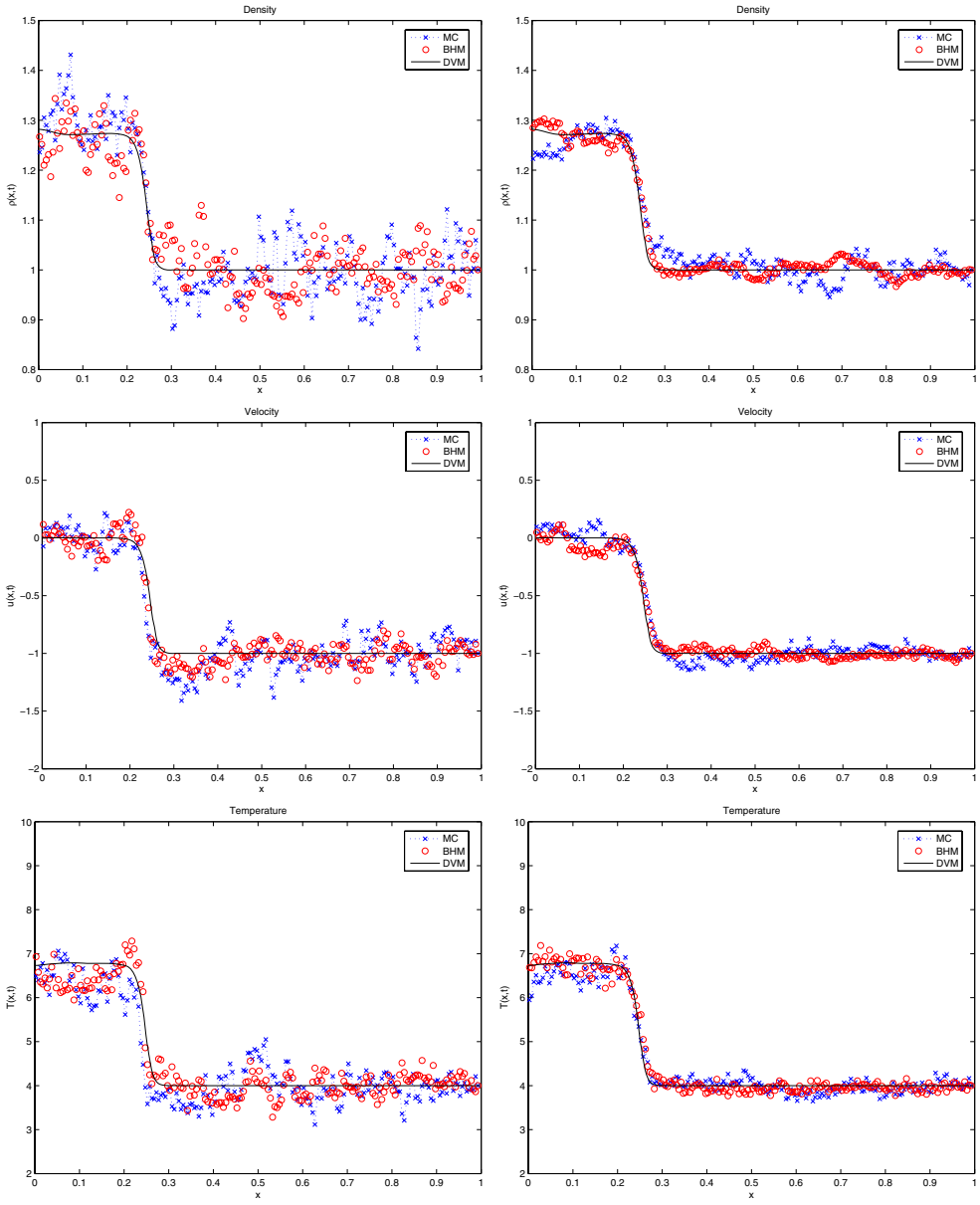

FIG. 10. *Unsteady shock: Solution at* $t = 0.065$ *with* $\varepsilon = 10^{-3}$ *for density (top), mean velocity (middle), and temperature (bottom) for MCM and BHM (left), BHMI and BCHM (right), with initial data* (87).

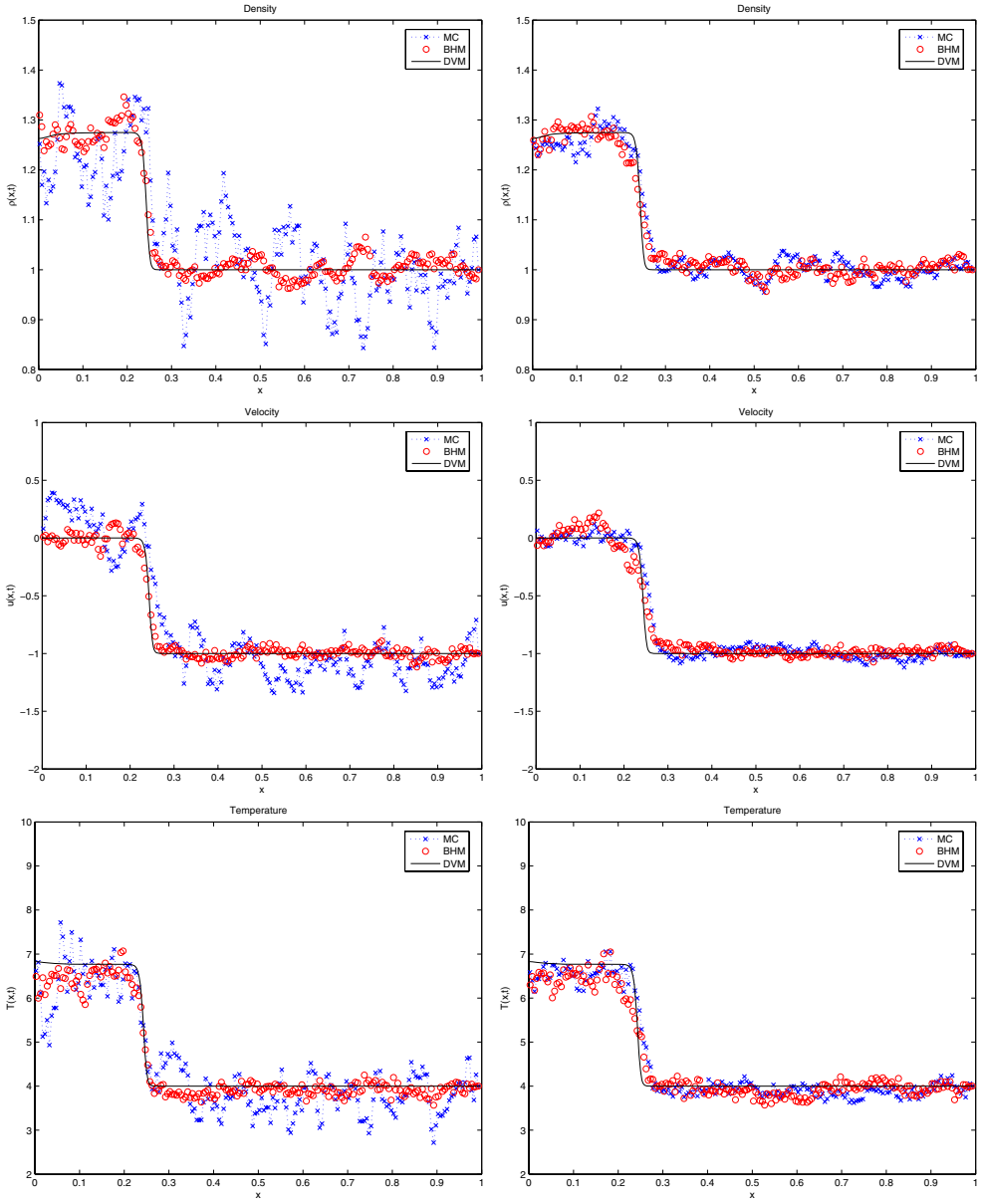

FIG. 11. *Unsteady shock: Solution at* $t = 0.065$ *with* $\varepsilon = 10^{-5}$ *for density (top), mean velocity (middle), and temperature (bottom) for MCM and BHM (left), BHMI and BCHM (right), with initial data* (87).

REFERENCES

[1] K. AOKI, Y. SONE, AND T. YAMADA, *Numerical analysis of gas flows condensing on its plane condensed phase on the basis of kinetic theory*, Phys. Fluids A, 2 (1990), pp. 1867–1878.

[2] G. A. BIRD, *Molecular Gas Dynamics and Direct Simulation of Gas Flows*, Clarendon Press, Oxford, UK, 1994.

[3] J. F. BOURGAT, P. LETALLEC, B. PERTHAME, AND Y. QIU, *Coupling Boltzmann and Euler equations without overlapping*, in Domain Decomposition Methods in Science and Engi-

neering, Contemp. Math. 157, AMS, Providence, RI, 1994, pp. 377–398.
[4] J. F. Bourgat, P. LeTallec, and M. D. Tidriri, *Coupling Boltzmann and Navier-Stokes equations by friction*. J. Comput. Phys., 127 (1996), pp. 227–245.
[5] R. E. Caflisch, S. Jin, and G. Russo, *Uniformly accurate schemes for hyperbolic systems with relaxation*, SIAM J. Numer. Anal., 34 (1997), pp. 246–281.
[6] R. E. Caflisch, H. Chen, E. Luo, and L. Pareschi, *A hybrid method that interpolates between DSMC and CFD*, in Proceedings of the 44th AIAA Aerospace Sciences Meeting and Exhibit, 2006, submitted.
[7] D. Calhoun and R. J. LeVeque, *An accuracy study of mesh refinement on mapped grids*, in Proceedings of the Chicago Workshop on Adaptive Mesh Refinement Methods, Lect. Notes Comput. Sci. Eng. 41, Springer-Verlag, Berlin, 2003, pp. 91–102.
[8] F. Coron and B. Perthame, *Numerical passage from kinetic to fluid equations*, SIAM J. Numer. Anal., 28 (1991), pp. 26–42.
[9] N. Crouseilles, P. Degond, and M. Lemou, *A hybrid kinetic-fluid model for solving the gas-dynamics Boltzmann BGK equation*, J. Comput. Phys., 199 (2004), pp. 776–808.
[10] P. Degond, G. Dimarco, and L. Mieussens, *A moving interface method for dynamic kinetic-fluid coupling*, J. Comput. Phys., submitted.
[11] P. Degond and S. Jin, *A smooth transition model between kinetic and diffusion equations*, SIAM J. Numer. Anal., 42 (2005), pp. 2671–2687.
[12] P. Degond, S. Jin, and L. Mieussens, *A smooth transition between kinetic and hydrodynamic equations*, J. Comput. Phys., 209 (2005), pp. 665–694.
[13] G. Dimarco and L. Pareschi, *Hybrid multiscale methods* I. *Hyperbolic relaxation problems*, Commun. Math. Sci., 4 (2006), pp. 155–177.
[14] G. Dimarco and L. Pareschi, *Domain decomposition techniques and hybrid multiscale methods for kinetic equations*, in Proceedings of the Eleventh International Conference on Hyperbolic Problems: Theory, Numerics, Applications, 2006, to appear.
[15] G. Dimarco and L. Pareschi, *A Fluid Solver Independent Hybrid Method for Multiscale Kinetic equations*, preprint, 2007.
[16] W. E and B. Engquist, *The heterogeneous multiscale methods*, Commun. Math. Sci., 1 (2003), pp. 87–133.
[17] W. E and B. Engquist, *The heterogeneous multiscale method for homogenization problems*, in Multiscale Methods in Science and Engineering, Lect. Notes Comput. Sci. Eng. 44, Springer-Verlag, Berlin, 2005, pp. 89–110.
[18] W. E and B. Engquist, *Multiscale modeling and computation*, Notices Amer. Math. Soc., 50 (2003), pp. 1062–1070.
[19] M. Jansen, R. Baraniuk, and S. Lavu, *Multiscale approximation of piecewise smooth two-dimensional functions using normal triangulated meshes*, Appl. Comput. Harmon. Anal., 19 (2005), pp. 92–130.
[20] S. Jin and C. D. Levermore, *Numerical schemes for hyperbolic conservation laws with stiff relaxation terms*, J. Comput. Phys., 126 (1996), pp. 449–467.
[21] S. Jin, L. Pareschi, and G. Toscani, *Diffusive relaxation schemes for multiscale discrete-velocity kinetic equations*, SIAM J. Numer. Anal., 35 (1998), pp. 2405–2439.
[22] S. Jin, L. Pareschi, and G. Toscani, *Uniformly accurate diffusive relaxation schemes for multiscale transport equations*, SIAM J. Numer. Anal., 38 (2000), pp. 913–936.
[23] M. A. Katsoulakis, A. J. Majda, and A. Sopasakis, *Multiscale couplings in prototype hybrid deterministic/stochastic systems.* I. *Deterministic closures*, Commun. Math. Sci., 2 (2004), pp. 255–294.
[24] M. A. Katsoulakis, A. J. Majda, and A. Sopasakis, *Multiscale couplings in prototype hybrid deterministic/stochastic systems.* II. *Stochastic closures*, Commun. Math. Sci., 3 (2005), pp. 453–478.
[25] P. LeTallec and F. Mallinger, *Coupling Boltzmann and Navier-Stokes by half fluxes*, J. Comput. Phys., 136 (1997), pp. 51–67.
[26] L. Mieussens, *Discrete velocity model and implicit scheme for the BGK equation of rarefied gas dynamic*, Math. Models Methods Appl. Sci., 10 (2000), pp. 1121–1149.
[27] K. Nanbu, *Direct simulation scheme derived from the Boltzmann equation*, J. Phys. Soc. Japan, 49 (1980), pp. 2042–2049.
[28] L. Pareschi and R. E. Caflisch, *Implicit Monte Carlo methods for rarefied gas dynamics* I: *The space homogeneous case*, J. Comput. Phys., 154 (1999), pp. 90–116.
[29] L. Pareschi and R. E. Caflisch, *Towards a hybrid method for rarefied gas dynamics*, in Transport in Transition Regimes, IMA Vol. Math. Appl. 135, Springer-Verlag, New York, 2004, pp. 57–73.
[30] L. Pareschi and S. Trazzi, *Numerical solution of the Boltzmann equation by time relaxed*

Monte Carlo (TRMC) methods, Internat. J. Numer. Methods Fluids, 48 (2005), pp. 947–983.

[31] L. Pareschi, *Hybrid multiscale methods for hyperbolic and kinetic problems*, in ESAIM Proceedings, Vol. 15, T. Goudon, E. Sonnendrucker, and D. Talay, eds., EDP Sciences, Les Ulis Cedex A, France, 2005, pp. 87–120.

[32] R. B. Pember, J. B. Bell, P. Colella, and W. Y. Crutchfield, *An adaptive Cartesian grid method for unsteady compressible flow in irregular regions*, J. Comput. Phys., 120 (1995), pp. 278–304.

[33] S. Pieraccini and G. Puppo, *Implicit-explicit schemes for BGK kinetic equations*, J. Sci. Comput., 32 (2007), pp. 1–28.

[34] R. Roveda, D. B. Goldstein, and P. L. Varghese, *Hybrid Euler/direct simulation Monte Carlo calculation of unsteady slit flow*, AIAA J. Spacecraft Rockets, 37 (2000), pp. 753–760.